1 2 Estimating the seasonal impact of optically significant water constituents on surface heating rates in the Western Baltic Sea

3 Bronwyn E. Cahill[1,2], Piotr Kowalczuk[3], Lena Kritten[2], Ulf Gräwe[1], John Wilkin[4] and Jürgen
4 Fischer[2]

5 [1]Physical Oceanography and Instrumentation, Leibniz Institute for Baltic Sea Research, Warnemünde 18119, Germany
6 [2]Institute of Meteorology, Free University Berlin, Berlin 12165, Germany
7 [3]Institute of Oceanology PAS, Powstańców Warszawy 55, 81-712 Sopot, Poland
8 [4]Department of Marine and Coastal Sciences, Rutgers University, New Brunswick, 08901 NJ, USA

9 *Correspondence to*: Bronwyn E. Cahill (bronwyn.cahill@io-warnemuende.de)

10 **Abstract.** Heating rates induced by optically significant water constituents (OSCs), e.g. phytoplankton and coloured

11 dissolved organic matter (CDOM), contribute to the seasonal modulation of thermal energy fluxes across the ocean-

12 atmosphere interface in coastal and regional shelf seas. This is investigated in the Western Baltic Sea, a marginal sea

13 characterised by considerable inputs of freshwater carrying nutrients and CDOM, and complex bio-optical and

14 hydrodynamic processes. Using a coupled bio-optical-ocean model (ROMS-Bio-Optic), the inherent optical properties

15 of different OSCs are modelled under varying environmental conditions and the underwater light field is spectrally-

16 resolved in a dynamic ocean. We estimate the relative contribution of these OSCs to the divergence of the heat flux and

17 heating rates and find that phytoplankton dominates the OSC contribution to heating in spring and summer, while

18 CDOM dominates in summer and autumn. The study shows that seasonal and spatial changes in OSCs in the Western

19 Baltic Sea have a small but noticeable impact on radiative heating in surface waters and consequences for the exchange

20 of energy fluxes across the air-sea interface and the distribution of heat within the water column. In the Pomeranian

21 Bight, where riverine influx of CDOM is strongest, water constituent-induced heating rates in surface waters in 2018

22 are estimated to be between 0.8 and 0.9 K m^{-1} d^{-1} in spring and summer, predominantly as a result of increased

23 absorption by phytoplankton and CDOM. Further offshore, OSC-induced heating rates during the same periods are

24 estimated to be between 0.4 and 0.8 K m^{-1} d^{-1}. Warmer surface waters are balanced by cooler subsurface waters. Surface

25 heat fluxes (latent, sensible and longwave) respond to warmer sea surface temperatures with a small increase in heat

26 loss to the atmosphere of 5 Wm^{-2} during the period April to September. We find relatively good agreement between our

27 modelled water constituent absorption, and in situ and satellite observations. More rigorous co-located heating rate

28 calculations using an atmosphere-ocean radiative transfer model provide evidence of the suitability of the ROMS-Bio-

29 Optic model for estimating heating rates.

30 1 Introduction

31 Radiant energy fluxes impact biological production in the ocean and are modulated in turn as a result of biological

32 production. This has fundamental consequences for upper ocean physics, surface nutrient supply, net primary and export

33 production and the exchange of soluble gases across the air-sea interface into the marine atmospheric boundary layer.

34   The contribution of optically significant water constituents (OSCs) to heating rates in the upper ocean is connected to

35   net primary and export production, through the direct effect of temperature on metabolic rates of marine plankton and

36   increased stratification and reduced vertical exchange of nutrients. This plays an important role in controlling the flow

37   of carbon and energy through pelagic systems (Wohlers et al., 2009; Taucher and Oschlies, 2011), in particular, the

38   partitioning between particulate and dissolved organic carbon, the transfer of primary produced organic matter to higher

39   trophic levels, the efficiency of the biological carbon pump and the exchange of CO_2 across the air-sea interface. Shelf

40   seas and coastal waters are characterised often by highly variable presence of inorganic suspended particulate matter

41   and coloured dissolved organic matter (CDOM). CDOM is the fraction of dissolved organic matter (DOM) that absorbs

42   light in natural waters in parts of the ultraviolet and visible spectral ranges (c. 200 - 550 nm). It is present throughout

43   the world oceans, both open and deep waters, and in coastal and shelf seas. It significantly contributes to the attenuation

44   of light in natural waters and thereby impacts ocean heat content, in particular in coastal and shelf seas (Soppa et al.,

45   2019; Gnanadesikan et al., 2019; Kim et al., 2015, 2016, 2018; Hill , 2008). In the Baltic Sea, CDOM is prevalent and

46   displays strong seasonal and spatial variability (Kowalczuk, 1999; Kowalczuk et al., 2006). Sources of CDOM and

47   changes to its composition through non-conservative processes are tightly coupled to the underwater light field. These

48   will vary with environmental conditions and phytoplankton community structure. Moreover, heterogeneity in

49   phytoplankton pigments and other water constituents will have implications for sub-mesoscale vertical mixing and

50   advective fluxes, and thus water temperature, density and the supply of nutrients to the surface. Understanding how the

51   variable presence of water constituents impacts energy fluxes in the upper ocean and across the air-sea interface, and the

52   accumulative effect on the upper ocean heat budget in shelf seas and coastal waters is of particular importance for our

53   capacity to adequately model regional ocean climate.

54   A number of feedback mechanisms determine the biogeochemical dynamics in the upper ocean layer. Solar

55   radiation penetrating the water column is scattered and absorbed by pure water, as well as by dissolved and particulate

56   water constituents. Absorbed radiation is mostly transformed into heat and thus directly controls heating rates and

57   subsequently impacts the vertical stratification of the euphotic layer. A portion of the light absorbed by autotrophic

58   protists is used for photosynthesis and consequently contributes to biomass production. The vertical distribution of

59   absorbing material may be altered significantly due to biogenic (and in coastal areas, non-biogenic) processes (e.g. by

60   the development of a subsurface algae bloom) which in turn leads to a significant change of the depth range at which

61   heating occurs (e.g. increased heating within the algae layer) and the availability of light (e.g. strongly reduced light

62   availability below the algae layer).

63   Biogeochemical dynamics are especially complex in shelf and coastal waters where organic and inorganic

64   particulate matter as well as CDOM may be present in individually highly varying concentration ranges, e.g. caused by

65   riverine inputs or sediment resuspension from the seafloor. For example, accounting for the highly variable light

66   attenuation in turbid river plumes is critical if nearshore physics are to be resolved correctly (Cahill et al., 2008; Kim et

67   al., 2020). Changes in surface temperature and buoyancy-driven circulation have important consequences for the

68 development, transport and fate of phytoplankton biomass. The resulting carbon fluxes across the air-sea interface,

69 exported to the benthos or advected off the shelf system are key to understanding the carbon budgets of shelf systems

70 and the open ocean.

1.1 Ocean radiant heating and biological production

72 For studies of heat transfer modulated by biological production in the upper ocean, it is important to accurately

73 prescribe the shortwave solar radiation in the upper water column. Downward solar radiation penetrating into the upper

74 ocean can be partitioned into three spectral domains: Visible (UV/VIS): ~0.30 µm - ~0.75 µm; Near Infrared (NIR):

75 ~0.75 µm - ~1.3 µm; Shortwave Infrared (SWIR): ~1.3 µm - ~3.5 µm. SWIR radiant energy plays an important role in

76 the surface thermal structure of the water column, however, its attenuation can be considered as invariable to changes of

77 water constituents (Morel and Antoine, 1994) as it is almost completely dominated by water absorption and is fully

78 attenuated very close to the sea surface. NIR radiant energy penetrates a bit deeper into the ocean but is still almost

79 entirely absorbed within the topmost one meter layer due to the still strong absorption of pure sea water at these

80 wavelengths. In contrast to that, the (spectral) attenuation of UV/VIS radiant energy within the water body is strongly

81 dependent on the presence of water constituents and may therefore vary considerably horizontally and vertically. More

82 specifically, the variability of UV/VIS in the water column is determined by absorption and scattering of three

83 substance classes: phytoplankton, CDOM and inorganic suspended sediment (Sathyendranath et al., 1989). Radiant

84 energy within the visible range is also harvested by autotrophic protists for photosynthesis purposes.

85 Biogeochemical dynamics in productive waters are characterized by the feedbacks between the absorption of

86 light by dissolved and particulate material and the corresponding ocean radiant heating in the upper water column. This

87 has been elegantly demonstrated for the open ocean where the upper ocean chlorophyll concentration regulates the

88 radiant transmission and heating rates in the mixed layer depth (Lewis et al., 1990; Morel and Antoine, 1994; Ohlmann

89 et al., 1996, 1998, 2000a, b; Murtugudde et al., 2002; Oschlies, 2004; Manizza et al., 2005, 2008). Enhanced near-

90 surface stratification has a positive feedback on phytoplankton growth by restricting phytoplankton within shallower

91 mixed layers with more available light, which in turn increases near surface local heating (Dickey and Falkowski, 2002).

92 Ohlmann et al. (2000) demonstrated that an increase in chlorophyll concentration from 0.03 mg m^{-3} to 3 mg m^{-3} in the

93 upper 10 m of the water column can decrease the solar flux in the waters below by as much as 35 Wm^{-2}. A 10 Wm^{-3}

94 change in the solar radiation absorbed within a 10 m layer can represent a temperature change within that layer of more

95 than 0.6°C month^{-1} (Simpson and Dickey, 1981). Löptien and Meier (2011) show that increased water turbidity affects

96 the summer sea surface temperature trends in the Baltic Sea significantly.

1.2 Biogeochemical ocean models

98 Despite these findings, coupled ecosystem-circulation models rarely share the same parameterization or source of

99 radiative forcing to drive the hydrodynamics and fuel photosynthesis even though their requirements for information on

100 light and heat overlap. This is in part due to the fact that historically, circulation and ecosystem models have evolved

101 independently and it is only in the last 10 to 15 years that coupling between the two has made significant advances. It is

102 typical that the ecosystem model is "plugged" into a circulation model and communication between the two is in one

103 direction only: state variables (such as temperature) computed in the circulation model are communicated to the

104 biological model at each time step, however, any change to the radiative fluxes as a consequence of biological activity

105 is not necessarily accounted for or communicated back to the circulation model so that potentially available

106 "information" related to heat transfer in the upper ocean and across the ocean-atmosphere interface is not being used.

107 Many parameterizations of the subsurface vertical distribution of shortwave solar radiation have evolved over the last

108 years (e.g. Paulson and Simpson, 1977; Zaneveld and Spinrad, 1980; Simpson and Dickey, 1981; Morel, 1988; Morel

109 and Antoine, 1994; Ohlmann and Siegel, 2000). The most common formulation of radiative forcing in bio-physical

110 models is one directional (i.e. assuming horizontal homogeneity) where radiative transfer is approximated by vertically

111 attenuating the net surface shortwave radiation by an exponential function based on Beer-Lambert Law (Paulson and

112 Simpson, 1977:

113

114 $$I_z = I_{IR} \cdot e^{-k_{IR}z} + I_{VIS} \cdot e^{-k_{VIS}z} \qquad (1)$$

115

116   The total surface irradiance is split into two wavebands corresponding to infrared (IR) and visible (VIS), and

117 the attenuation coefficients, k, for both the IR and VIS parts of the spectrum are prescribed according to different Jerlov

118 (1976) water types. For photosynthesis purposes, one of the more simple parameterizations of light attenuation is based

119 on the surface photosynthetically available radiation (PAR) computed as a fraction of the net surface solar flux

120 (typically 43%) and then attenuated through the water column as a function of chlorophyll concentration (e.g. Fennel et

121 al., 2006, 2008; Fennel and Wilkin, 2009). A further level of complexity may be introduced by splitting the visible

122 portion of the light spectrum into two wavebands (red and blue/green) and computing the diffuse attenuation

123 coefficients, k, for the two wavebands as a function of modelled chlorophyll concentration after Morel (1988) as

124 described by Manizza et al. (2008):

125

126 $$I_z = I_{IR} \cdot e^{-k_{IR}z} + I_{RED(z-1)} \cdot e^{-k_{RED}\Delta z} + I_{BLUE(z-1)} \cdot e^{-k_{BLUE}\Delta z} \qquad (2)$$

127

128   This chlorophyll-based approach is reasonably accurate for the open ocean where phytoplankton dominates the

129 inherent optical properties of the water constituents (Morel and Prieur, 1977); however, it is inadequate in shelf and

130 coastal oceans as it neglects important contributions from CDOM and suspended sediments. More recently, Neumann et

131 al. (2015) show that, in the Baltic Sea, including more water constituents in the estimation of light attenuation in their

132 model yields a more realistic representation of the light climate, and improved estimates of primary productivity, Secchi

133 disk depth and oxygen concentrations. They estimate K(PAR) by explicitly accounting for modelled phytoplankton

biomass, detritus, dissolved organic matter due to metabolism and degradation processes, and parameterizing CDOM as a function of salinity, as follows:

$$K_{PAR} = k_w + k_c Chl + k_{det} DET + k_{don} DON + k_{CDOM}(S) \qquad (3)$$

where k_w [m^{-1}] is the attenuation coefficient of water, k_c, k_{det}, and k_{don} [(mg N)$^{-1}$m^2] are the nitrogen-specific attenuation coefficients of chlorophyllouse particles, detritus, and dissolved organic matter, respectively and Chl, DET, and DON [mg N m^{-3}] are the concentrations of phytoplankton biomass, detritus, and dissolved organic matter due to metabolism and degradation processes, respectively. k_{CDOM} [m^{-1}] is the attenuation coefficient of dissolved organic substance transported by rivers with fresh water into the estuary and S is salinity.

More recently, Neumann et al. (2021) explicitly consider light absorption due to terrestrial CDOM in their ecosystem model of the Baltic Sea, using earth observation CDOM absorption data from Sentinel-2 MSI as a proxy for terrestrial sources of CDOM. They show a significant improvement in CDOM estimates in particular in the northern parts of the Baltic Sea where the impacts of terrestrial CDOM are large.

A few studies have tried to explore the full biophysical feedbacks using coupled physical-biological ocean models (Oschlies, 2004; Manizza et al., 2005; 2008) and fully coupled atmosphere-bio-physical ocean model (Jolliff and Smith, 2014; Wetzel et al., 2006). Notably, results from Oschlies (2004) include a net cooling of the North Atlantic by biota of about 1 Wm^{-2}, with enhanced upper ocean stratification in summer and deeper winter mixed layer depths (> 100 m) in parts of the subpolar gyre. Coastal upwelling and associated nutrient supply is reduced, especially in coastal upwelling regions of West Africa. Overall, there is a negative feedback of biotically induced radiative heating on chlorophyll-a concentrations, except in parts of the subpolar North Atlantic where intensification of the spring bloom results in increased annual mean chlorophyll-a concentrations. Wetzel et al. (2006) further highlighted the importance of marine biology on the radiative budget of the upper ocean, and found positive feedbacks with the climate system cause a global shift of the seasonal cycle, with the onset of spring occurring about two weeks earlier. Increased wind stress and changes in the shortwave radiation led to significant warming in the mid latitudes in summer and to seasonal modifications of the overall warming in the equatorial Pacific. Jolliff and Smith (2014) demonstrated a regional example of biological modulation of upper ocean physics in Monterey Bay, California and show how the spatiotemporal pattern of a phytoplankton bloom can persists because of enhanced thermal stratification promoting vertical stability and more efficient use of macronutrients. Furthermore, biothermal warming of surface waters modifies the local surface pressure gradient and modulates wind stress patterns.

More recent studies which investigate the role of OSCs and surface heating, highlight the role of CDOM in Arctic amplification (e.g. Soppa et al., 2019; Pefanis et al., 2020) and the impact of CDOM on the annual cycle of sea surface temperature in coastal and northern subpolar regions (Gnanadesikan et al., 2019; Kim et al., 2015; 2016; 2018). Soppa et al. (2019) found that a CDOM absorption at 443 nm of 1.77 m^{-1} contributed to an increased radiative heating

168   of 0.6°C d⁻¹ in the upper 2 m in the Laptev Sea shelf waters, implying increased sea ice melt rates and changes in the

169   surface heat fluxes to the atmosphere. Pefanis et al. (2020) confirm that increases in CDOM in the Arctic amplify

170   surface warming by increasing surface temperatures in summer and decreasing sea-ice concentrations. They also show

171   that summertime surface warming associated with increases in CDOM induces more heat loss to the atmosphere,

172   primarily through latent and sensible heat fluxes. Gnanadesikan et al. (2019) demonstrate that the presence of CDOM

173   leads to an increase in the amplitude of the seasonal cycle of SST over coastal and northern subpolar regions, with

174   potential implications for extreme ocean temperatures. Importantly, they find the size and sign of the change in

175   amplitude are controlled by the interplay between enhanced surface shortwave heating, shading and cooling of the

176   subsurface and the extent to which these are connected by vertical mixing. They show that the interplay between heat

177   term balances varies regionally. In the central Baltic Sea (58°N, 19.5°E), changes in the seasonal cycle of the heat

178   budget are explained by a 1D balance between the penetration of shortwave radiation and vertical mixing (see Figure 3a

179   in Gnanadesikan et al., 2019) with advective and diffusive terms being relatively small. In other regions around the

180   world, the heat term balance is represented by a more complicated interplay between the penetration of shortwave

181   radiation, vertical and horizontal mixing and advection (see Figure 3b, c, d in Gnanadesikan et al., 2019).

182   Lastly, Skákala et al. (2022) demonstrate a significant impact of biogeochemistry on physics in the North West

183   European Shelf, with the light attenuation by chlorophyll being responsible for a 1 °C warming in the upper 20 m of the

184   ocean with comparable cooling taking place between 20 and 200 m. They also show that accounting for this water

185   constituent-induced heating improves the timing of the simulated phytoplankton bloom in the region.

186   In this work, we examine the relationship between OSCs, in particular, CDOM, phytoplankton and detritus,

187   and heating rates in the Western Baltic Sea. High concentrations of CDOM optically distinguish the Baltic Sea from

188   other coastal seas (Simis et al., 2017), making it an interesting study site for this application. CDOM also exhibits

189   strong seasonal and spatial variability in the region which is dependent on sources of CDOM and physics, e.g. periods

190   of intensive mixing and high riverine discharge versus periods of thermal stratification, reduced riverine discharge,

191   enhanced biological production and production of CDOM (Kowalczuk, 1999; Kowalczuk et al, 2005a). In this study,

192   we examine precisely this interplay between physics and OSCs using an integrated analysis framework. This consists of

193   a coupled bio-optical ocean model which incorporates the optical properties of key water constituents and explicitly

194   resolves sources of both terrestrial and authochthonous CDOM as a state variable in a 4D ocean state. We model the

195   inherent optical properties of different water constituents under varying environmental conditions and spectrally resolve

196   the underwater light field in a dynamic ocean. From this, we estimate the contribution of key water constituents to

197   surface heating rates and feedbacks with the marine atmospheric boundary layer heat fluxes. We evaluate our estimates

198   of surface heating rates using an ocean-atmosphere radiative transfer model and optical measurements from in situ and

199   remote sensing observations.

2 Methods

2.1 Study site

Kowalczuk et al. (2006) have shown that there are three pools of CDOM in the waters of the Southern Baltic Sea: a riverine pool, an aged marine pool and a pool primarily produced in offshore waters. They explored the seasonal dependence between the light absorption coefficient of CDOM at 375 nm, aCDOM(375), and salinity and chlorophyll-a concentrations in the Southern Baltic Sea and found a seasonal dependence between physical processes and the source of CDOM. In March, April and November, months of intensive mixing and high riverine discharge, most of the variability in aCDOM(375) values could be explained by dilution of terrestrially derived CDOM alone. In February, May and September, months of thermal stratification, reduced riverine discharge and enhanced biological activity, autochthonous production of CDOM was found to be a significant source of CDOM in the Southern Baltic Sea. Changes in the values of spectral slope coefficients are regarded as an indicator of compositional changes in CDOM. These changes can be a result of either conservative mixing processes, i.e. mixing, or non-conservative processes, e.g. production, degradation or flocculation (Kowalczuk et al., 2006).
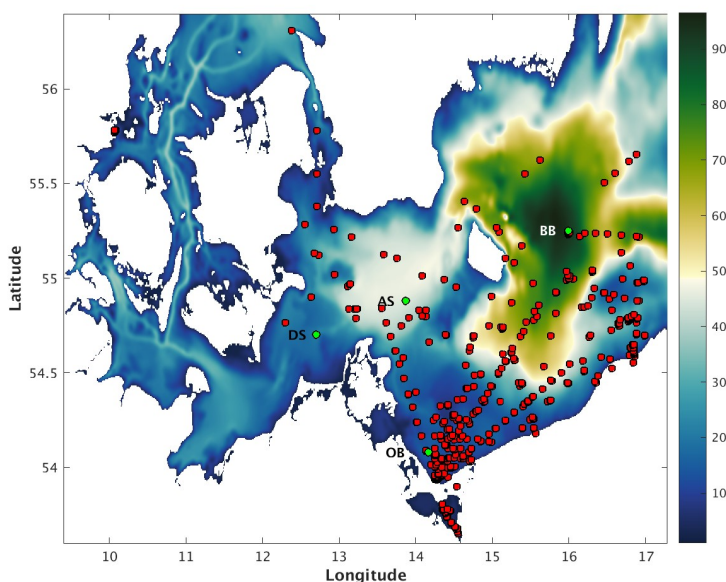
Figure 1: Western Baltic Sea model domain bathymetry (m) with location of model output analysis stations, Darß Sill (DS), Arkona Sea (AS), Oder Bank (OB) and Bornholm Basin (BB) (green dots) and in situ CDOM and NAP (non-algal particle) absorption measurements from the Institute of Oceanology of the Polish Academy of Sciences, IOPAN (red dots).

220

221 Our study site in the Western Baltic Sea (Figure 1) includes the Bornholm Basin, where we expect the seasonal cycle to

222 be explained by a 1D balance between the penetration of shortwave radiation and vertical mixing (Gnanadesikan et al.,

223 2019), and the Darß Sill, Arkona Sea and Oder Bank, where advection and diffusion will also contribute to the seasonal

224 heat balance, making for an interesting contrast between local regimes. At the Bornholm Basin, we expect to find

225 marine CDOM, at the Darß Sill and Arkona Sea, we expect to find a mixture of riverine and marine CDOM, depending

226 on the season, while at the Oder Bank, we expect the CDOM pool to be dominated by riverine sources from multiple

227 inlets and rivers connecting the Oder River outlet through Szczecin Lagoon with the Greifswalder Bodden and the

228 coastal Baltic Sea (Kowalczuk et al., 1999).

229 **2.2 Theory**

230 Light penetrating a water body can be described as consisting of three streams (Aas, 1987; Ackleson et al., 1994; Gregg,

231 2002 and Dutkiewicz et al., 2015). These are the downward direct irradiance, E_{dir}, the downward diffuse irradiance, E_{diff}

232 and the upward diffuse irradiance, E_u. $E_{dir} + E_{diff}$ is commonly referred to as downward irradiance, E_d. For studies of

233 heat transfer and photosynthesis, we need to know the scalar irradiance, E_0 which describes the light field integrated

234 over a sphere, and is thus independent of direction. All of these irradiance quantities (E_{dir}, E_{diff}, E_u and E_0) are a function

235 of wavelength and depth.

236 Following Morel (1988), the rate of radiant energy converted into heat can be estimated as follows:

237

238 $$\frac{dT}{dt} = -\frac{d(E_d - E_u)}{dz}\frac{1}{\rho C_p}$$ (4)

239

240 where the first term on the right hand side is the heat flux, E_d and E_u are the downward and upward irradiances,

241 respectively, ρ is the in situ density and C_p is the specific heat capacity of water. In a horizontally homogeneous water

242 body, the divergence of the radiative flux can be approximated as follows (Morel, 1988):

243

244 $$\frac{d(E_d - E_u)}{dz} \cong -aE_0 \approx K_d E_d$$ (5)

245

246 where a is the local absorption coefficient, E_0 is the scalar irradiance at the depth in question and K_d is the

247 downward diffuse attenuation coefficient for downwelling irradiance. These quantities are all dependent on depth,

248 concentrations of OSCs (e.g. phytoplankton pigments, CDOM, detritus) and wavelength. Thus,

249

250 $$\frac{dT}{dt} = -\frac{\int_{400}^{700}[E_d(\lambda, z).K_d(\lambda, z)]d\lambda}{\rho C_p}$$ (6)

251

252   K_d varies with both absorption, a, and scattering b, as well as with the angular distribution of the incoming

253   light field. It can be calculated from E_d, as follows (Gordon et al., 1980):

254

255     $$K_d = \frac{-d ln E_d(\lambda,z)}{dz} = \frac{-1}{E_d(\lambda,z)}\frac{d E_d(\lambda,z)}{dz} \qquad (7)$$

256

257   Biogeochemical-optical relationships vary significantly over different regions and/or seasons, therefore,

258   regional and temporal relationships have been adopted to cope with such variations when information concerning the

259   directionality of the underwater light field is limited. For example, in open ocean waters, where attenuation of

260   underwater light is primarily a function of chlorophyll concentration, Sathyendranath and Platt (1988) parameterize K_d,

261   as follows:

262

263     $$K_d = \frac{a+b}{\mu_0} \qquad (8)$$

264

265   where a is the absorption and b is the total scattering (forward and backscatter) of OSCs, while μ_0 is the

266   average cosine, which tells you how much the light field differs from isotropic conditions.

267   In more complex coastal waters, Lee et al. (2005) have derived an empirical algorithm to parameterize K_d, as

268   follows:

269

270     $$K_d = (1 + 0.005\theta)a(\lambda,z) + 4.18(1 - 0.52e^{-10.8a(\lambda,z)})b_b(\lambda,z) \qquad (9)$$

271

272   where θ is the solar zenith angle in degrees and b_b is the backscatter coefficient.

273   If the absorption and scattering properties of different water constituents are known, K_d can be estimated using

274   Eq. (8) or Eq. (9) and E_d can then be calculated using Eq. (10).

275

276     $$E_d = E_d(0)e^{-K_d z} \qquad (10)$$

277

278   Thus, the heat balance relationship described in Eq. (6), can be used to estimate heating rates.

279

280 2.3 Model system

281 2.3.1 Regional Ocean Modelling System, ROMS

282 The ocean model component, ROMS, is widely used for shelf circulation (e.g. Haidvogel et al., 2008, Wilkin et al.,

283 2011) and coupled physical-biological applications (e.g. Cahill et al., 2008; 2016, Fennel et al., 2006; 2008; 2013,

284 Fennel and Wilkin, 2009). The ROMS computational kernel (Shchepetkin and McWilliams, 2005) produces accurate

285 evolution of tracer fields, which is a particularly attractive feature for biogeochemical modelling because it facilitates

286 the correct interaction among tracers and accounting of total nutrient and carbon budgets. Within ROMS, we have

287 incorporated a novel spectrally-resolved bio-optical module, herein called Bio-Optic.

288 BioOptic is an adaptation of the carbon-based, ecological/optical modelling system Ecosim (Bissett et al.,

289 1999a, b) which was developed for simulations of carbon cycling and biological productivity. It simulates up to four

290 phytoplankton functional groups each with a characteristic pigment suite which varies with the group carbon-to-

291 chlorophyll-a ratio, C:Chla. The properties of each functional group evolve over time as a function of light and nutrient

292 conditions (i.e. NO_3, NH_4, PO_4, SiO and FeO). Marine and riverine sources of dissolved organic carbon (DOC and

293 CDOC) are accounted for and explicitly resolved into labile (e.g. available for biological and photo-degradation) and

294 relict (e.g. available for photo-degradation) forms. Dissolved inorganic carbon is also accounted for. Riverine sources of

295 carbon and nutrients are introduced via point sources. The underwater light field is spectrally-resolved between 400 and

296 700 nm, which allows for differential growth of different phytoplankton groups that have unique pigment complements.

297 The interaction between Ecosim's components describe autotrophic growth of and competition between phytoplankton

298 groups, differential carbon and nitrogen cycling, nitrogen fixation and grazing.

299 BioOptic builds on Ecosim's functionality as follows. The inherent optical properties (absorption, scatter and

300 backscatter) of each of the OSCs (i.e. phytoplankton, detritus and CDOM) are explicitly resolved and their individual

301 contribution to the downward attenuation and downward and scalar irradiance fields is calculated. The surface solar

302 downwelling spectral irradiance, $E_d(\lambda,0-)$ and the average cosine zenith angle, $\mu_0(\lambda,0-)$, just beneath the sea surface, are

303 calculated according to Gregg and Carder (1990). This includes the impact of clouds, water vapour and aerosols in the

304 atmosphere and the surface roughness and reflectance at the ocean-atmosphere interface. Spectral irradiances between

305 400 and 700 nm are provided at 5 nm intervals. The downwelling irradiance attenuation coefficient, K_d, is calculated

306 following Eq. (9) after Lee et al. (2005). The spectrally-resolved downward light stream, $E_d(\lambda,z)$, which is calculated

307 according to Eq. (10), incorporates both direct and diffuse components of the light field and is attenuated by absorption,

308 a, and scattering, b (forward, b and backward, b_b) of phytoplankton, detritus and CDOM. The average cosine is

309 modified with depth as a function of absorption and backscattering, and the total scalar irradiance, $E_0(\lambda,z)$, which is the

310 light available to phytoplankton, is calculated following Eq. (5) after Morel (1988).

311 The explicit calculation of in-water spectrally-resolved absorption, scattering and backscattering coefficients,

312 average cosine, downwelling irradiance attenuation coefficient, K_d, in addition to the scalar, E_0, and downward, E_d,

313 irradiance fields, has important implications. The spectrally-resolved underwater light field drives the evolution of

OSCs in the ecosystem model, while the OSCs in turn determine the evolution of the light field in each layer by absorption and scattering of the light. This means that the OSCs' contribution to the divergence of the heat flux (Morel, 1988) can be accounted for within the full hydrodynamic solution. Furthermore, water constituent-induced heating rates can be assessed and their impact on the ocean sea surface temperature is communicated to the bulk flux formulation of the atmosphere in the modelling system.

While this still represents a very simplified treatment of radiative transfer with the water column, it does permit a direct evaluation of the optical terms and heating rates with those derived from a full solution of the radiative transfer equations and provides a means to improving the parameterization of water constituent-based heat flux algorithms in ocean models.

2.3.2 Vector radiative transfer model, MOMO

A more rigorous treatment of the vertical structure of the light field is provided by atmosphere-ocean radiative transfer models, such as MOMO (Fell and Fischer, 2001), which simulate the light field in the stratified atmosphere-ocean system for the VIS and NIR spectral ranges. MOMO uses the matrix operator method to calculate zenithally and azimuthally resolved light fields for different types and concentrations of optically active components in the ocean and atmosphere, thus, the full directionality of the light field is accounted for. The main advantage of the matrix-operator method is its efficiency in simulating light propagation in optically dense media. It is therefore particularly suited for the use in the development of remote sensing algorithms for the retrieval of water constituents. It is most recently described in Hollstein and Fischer (2012) and is based on previous work by Fischer and Grassl (1984) and Fell and Fischer (2001). It has been successfully applied to remote sensing of lakes (Heege and Fischer, 2004), analysis of hyperspectral, ocean colour data to derive surface fluorescence signals (Guanter et al., 2010), analysis of ocean color data from MERIS measurements (Zhang et al., 2003) and a new retrieval of sun-induced chlorophyll fluorescence in water from ocean colour measurements (Kritten et al., 2020). For our purposes, the most pertinent elements of MOMO include the calculation of the spectrally-resolved downward surface irradiance for the VIS and NIR ranges, the direct and diffuse downwelling and the diffuse upwelling components of the underwater light field.

2.4 Experimental setup

The ROMS Bio-Optic modelling system was configured for the Western Baltic Sea as described in Table 1. The model domain has a horizontal resolution of ~ 1.8km with 285 x 169 grid points in the horizontal, 30 sigma levels in the vertical, a bulk flux atmosphere forced with DWD-ICON output (Zängl et al., 2015) and river forcing including runoff and biogeochemistry derived from HELCOM PLC (Pollution Load Compilation) data (Neumann, pers. comm). Open boundaries to the north and east were forced with output from GETM physics (Gräwe et al., 2015a, b) using a combination of Chapman / Flather conditions for u and v velocities and transports, and Radiation + Nudging for temperature and salinity. This 3D setup is based on an existing GETM physics setup which has been previously

346 evaluated and published (Gräwe et al., 2015a,b). We focus our evaluation on the modelled inherent optical properties of

347 the water constituents using observations from Kowalczuk et al. (2005a,b) and Meler et al. (2016a,b).

348 We performed two experiments, as follows:

1. 3D Western Baltic Sea, feedback of constituent-induced heating into hydrodynamic solution (herein referred to as "biofeed")

2. 3D Western Baltic Sea, no feedback of constituent-induced heating into hydrodynamic solution (herein referred to as "nobiofeed")

353 The simulation period for both experiments was 2018.

354

355 **Table 1: Model configuration**

Model Configuration	
Components	3D Western Baltic Sea
Model Grid	285 x 169 (1nm), 30 sigma levels
Simulation Period	2018
Boundary Conditions	Chapman for zeta, Flather for ubar and vbar; Radiation + Nudging for temperature and salinity
Bulk Flux Atmosphere	DWD-ICON 3-hourly
River Forcing	HELCOM PLC (Pollution Load Compilation), Neumann (pers. comm.)
Initial Condition	GETM / ERGOM
Time Step	DT = 30s; NDTFAST = 20s
Evaluation	Water constituent absorption: • Kolwaczuk et al, 2005; Meler et al., 2016; MERIS Climatology Water constituent-induced heating rates: • Comparable MOMO full radiative transfer calculations at Bornholm Basin

356

357 MOMO simulations were performed over a range of solar zenith angles representative of seasons in the

358 Western Baltic Sea using phytoplankton, CDOM and detrital absorption and scattering coefficients modelled using

359 ROMS-Bio-Optic. Phase functions measured by Siegel et al. (2005) for various Baltic Sea coastal waters indicate that

360 the Baltic Sea in general has a relatively low backscatter. Seasonal heating rates were derived from ROMS-Bio-Optic at

361 the Bornholm Basin location and from comparable MOMO simulations in order to assess the suitability of the

362 simplified treatment of radiative transfer in ROMS-Bio-Optic and the implications of not resolving the full

363 directionality of the light field therein.

2.5 In situ and remotely sensed data

In situ observations and remotely sensed data from the MERIS ocean colour archive of CDOM absorption at 443 nm were used to develop a climatology of CDOM absorption with which to evaluate our modelled estimates of seasonal CDOM absorption. Below, the source and processing of the different data sets are briefly described.

2.5.1 In situ data

A time series (1994 - 2017) of in situ observations of CDOM absorption at 443 nm was reprocessed into seasonal means for our study area (Figure 1). This data set was collected as a result of the implementation of numerous research projects and statutory research programs conducted by the Remote Sensing Laboratory at the Institute of Oceanology, Polish Academy of Sciences (IOPAN), Sopot Poland in the whole Baltic Sea. The main aim of the study on CDOM optical properties was the assessment of its temporal and spatial variability (Kowalczuk and Kaczmarek, 1996, Kowalczuk, 1999) and its relation to hydrodynamic conditions and Baltic Sea productivity (Kowalczuk et al., 2006). As the primary goal of this research was the development and validation of ocean colour remote sensing algorithms (Kowalczuk et al., 2005a), the vast majority of samples for determination of CDOM absorption spectrum were collected in the surface layer. However, since 2014, samples were also collected within the water column, depending on the thermohaline stratification of water masses and depth distribution of autotrophic protists, in order to better resolve the impact of non-linear processes (i.e. photo-degradation, autochthonous production by phytoplankton, diffusion from bottom sediments) influencing CDOM optical properties (Kowalczuk et al., 2015). The sampling program is conducted in the whole Baltic Sea and is designed to resolve the spatial variability of the CDOM absorption coefficient. We use a subset of this time series located in our study area (Figure 1). Most of the samples were taken in spring and autumn, with a smaller number of samples collected in winter and summer mostly due to adverse weather conditions or unavailability of research vessels in summer months. Water samples were collected by Niskin bottle and were filtered first through acid-washed Whatman glass fibre filters (GF/F, nominal pore size 0.7 mm). The water was then passed through acid washed membrane filters with 0.2 mm pore to remove fine-sized particles. From 2014 until the present, water for CDOM absorption spectra were gravity filtered directly from Niskin bottles through Millipore Opticap XL4 Durapore filter cartridge with nominal pore size 0.2 μm. Filtered water was kept in acid washed amber glass 200 ml sample bottles until spectrophotometric analysis, which was performed with use of various models of bench top research grade, double beam spectrophotometers both in land base laboratory (Kowalczuk and Kaczmarek, 1996; Kowalczuk, 1999) and on the ship (Kowalczuk et al., 2005a,b, 2006). The cuvette pathlength was 5 or 10 cm depending on the spectrophotometer model. MilliQ water was used as the reference for all measurements. The absorption coefficient aCDOM(λ) was calculated using Eq. (11) as follows:

$$a_{CDOM}(\lambda) = \frac{2.303A(\lambda)}{L} \qquad (11)$$

397   where L is the optical path length, A is the absorptance (the flux that has been absorbed) and the factor 2.303 is the

398   natural logarithm of 10.

399   The whole CDOM absorption data base in the IOPAN repository, collected between 1994 and 2017, was

400   reprocessed to calculate the spectrum slope coefficient, S. A nonlinear least squares fitting method using a Trust-Region

401   algorithm implemented in Matlab was applied (Stedmon et al., 2000, Kowalczuk et al., 2006) in the spectral range 300-

402   600 nm, using Eq. (12) as follows:

403

404 $$a_{CDOM}(\lambda) = a_{CDOM}(\lambda_0)e^{-S(\lambda_0-\lambda)} + K \qquad\qquad (12)$$

405

406   where λ_0 is 350 nm, and K is a background constant that allows for any baseline shift caused by residual

407   scattering by fine size particle fractions, micro-air bubbles or colloidal material present in the sample, refractive index

408   differences between sample and the reference, or attenuation not due to CDOM. The parameters aCDOM (350), S, and

409   K were estimated simultaneously via non-linear regression using Eq. (12).

410   **2.5.2 Remotely sensed data**

411   MERIS FRS L2 (full resolution level 2) product from 2003 to 2012 was used to create a monthly climatology of CDOM

412   absorption for the Western Baltic Sea region. The MERIS FRS L2 product was processed with the C2RCC algorithm

413   (Doerffer and Schiller, 2007) which has been trained with data-sets from European coastal waters. Full details of the

414   post processing of the MERIS data into a climatology can be found in Röhrenbach (2019). A monthly climatology for

415   the complete time frame of the MERIS archive was created and includes the mean value, standard deviation and number

416   of observations for each point.

417
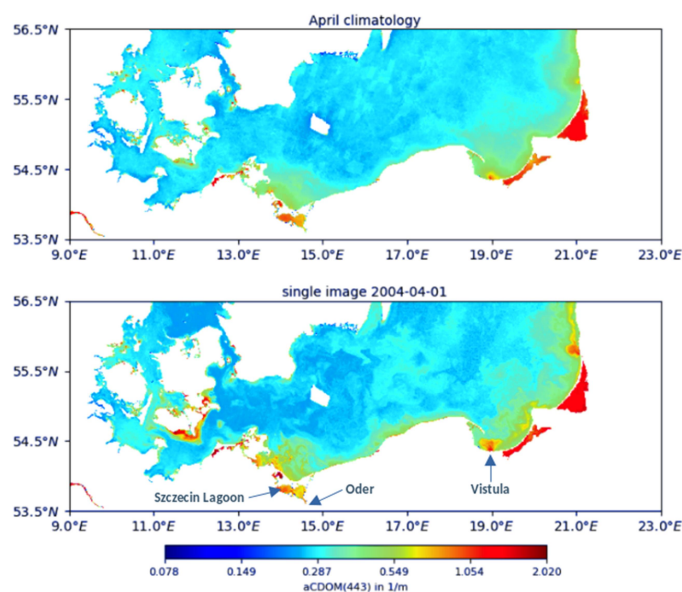
418
419

420   Figure 2: April climatology (top) and snapshot (01.04.2004) (bottom) of CDOM absorption at 443 nm (adapted from

421   Röhrenbach, 2019).

422

423   Figure 2 shows the difference between a snapshot of the MERIS data product (01.04.2004) and the

424   corresponding April climatology. The snapshot has almost complete data coverage, which is quite rare compared to

425   other time periods where only a small part of the region of interest is in the frame or free of cloud coverage. The

426   climatology smooths the spatial variability, providing the average spatial distribution and gradients in CDOM

427   absorption. High values of aCDOM(443) can be seen around the river mouths of the Vistula river (≈ 1.7 m^{-1}) and the

428   Oder river (≈ 0.7 m^{-1}), whereas offshore areas show lower values (≈ 0.2 m^{-1}) and spatial variability. The snapshot image

429   presents the typical situation at the beginning of the spring freshet. Both Vistula and Oder rivers have similar

430   hydrographic properties with maximum flow observed in April and May and minimum flow in June and February. The

431   land use in the catchment is also similar and consists of a mixture of agriculture, forestry and urbanised areas. The

432   difference in aCDOM(443) values and the spatial extent of fresh water plumes seen as areas with elevated CDOM

433   absorption results from the geomorphology of the outlets. The Vistula River has artificial outlets, built in 1895, and this

434   channel carries up to 90 % of the flow with only a small fraction feeding old deltaic branches, cut off by locks and dikes.

435   The Oder river outlet is less transformed by human activity, and the Oder River feeds the Szczecin Lagoon which is

436   connected to the coastal Baltic Sea via three inlets: two located in Poland (Swina and Dziwna) and one in Germany

437   (Peene). The shallow Szczecin Lagoon acts as a buffer and biogeochemical reactor, where photochemical, microbial and

438 physical (flocculation) transformation of CDOM may occur leading to effective decreased absorption values recorded

439 on the marine side of the estuary.

440 **3 Results**

441 In section 3.1, we show the results from the biofeed experiment which includes the feedback from OSC-induced heating

442 into the hydrodynamic solution. In section, 3.2 we show the difference between the biofeed experiment and the

443 nobiofeed experiment where no feedback from OSC-induced heating is included in the hydrodynamic solution.

444 **3.1 Seasonal cycle of temperature and the inherent and apparent optical properties of OSCs at Oder Bank, Darß**
445 **Sill, Arkona Sea and Bornholm Basin in Western Baltic Sea**

446 The modelled versus observed annual cycle of temperature at the different locations are shown in Figure 3. High

447 resolution temporal and vertically resolved observations for 2018 were only available at Darß Sill and Arkona Sea sites

448 (middle plots, Figure 3). Oder Bank and Darß Sill are shallow, well-mixed locations, where seasonal warming and

449 cooling of the whole water column takes place between May and October. At the deeper Arkona Sea and Bornholm

450 Basin locations, the onset of seasonal stratification sets in early May and starts to break down in late October. Intense

451 summertime warming late July, early August (SST ~ 25°C) leads to a deepening of the thermocline from c. 20 m to the

452 seafloor at Arkona Sea and to c. 38 m at Bornholm Basin. Overall, there is very good agreement between the modelled

453 biofeed results and observed temperature fields at all locations, especially the sea surface temperature (see Table 2 for r^2,

454 RMSE and BIAS statistics).

455
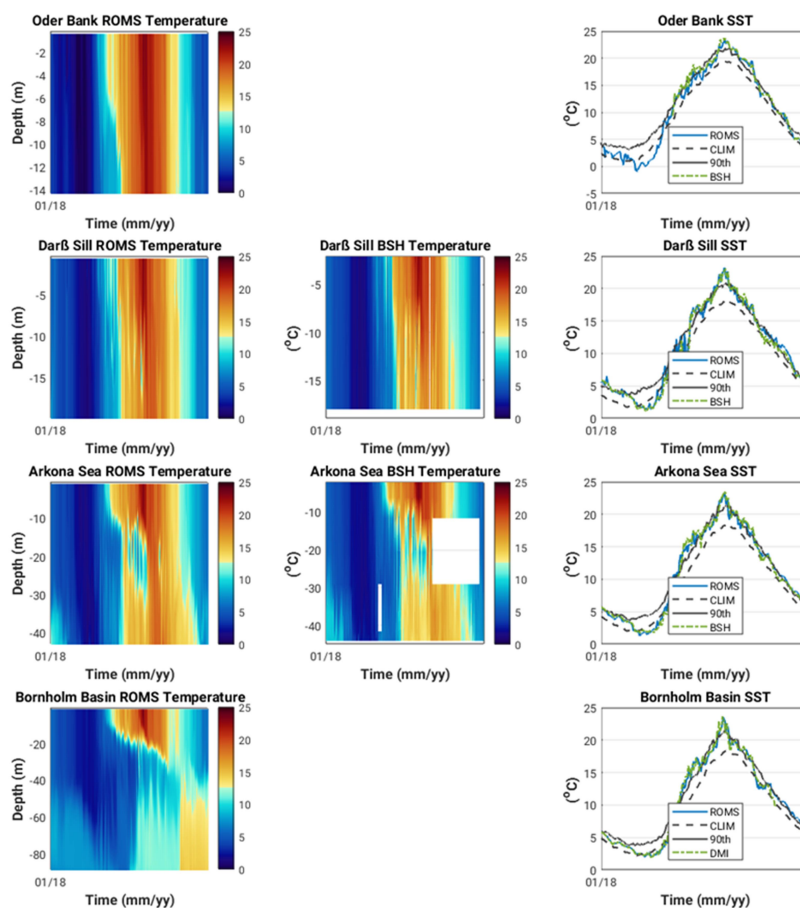
Figure 3: Modelled (left) versus observed (middle) annual cycle of temperature and sea surface temperature (right) in 2018 at Oder Bank, Darß Sill, Arkona Sea and Bornholm Basin. (see text for details).

This is especially important as 2018 was a year where two significant marine heat waves (defined as periods where the surface temperature exceeds the 90th percentile of the 30 year local mean for longer than 5 days) took place in May - June (38 days) and July – August (32 days). This result confirms the importance of accounting for the contribution of OSCs to the transfer of light energy.

467   **Table 2: Model versus observations statistics**

	r^2	RMSE	BIAS
Oder Bank	0.98	0.025	0.0017
Darß Sill	0.98	0.020	-0.0010
Arkona Sea	0.99	0.016	-0.0010
Bornholm Basin	0.99	0.005	0.0003

468

469   Modelled seasonal spectral surface absorption from the 3D Western Baltic Sea experiment for phytoplankton,

470   CDOM and detritus is shown for Oder Bank, Darß Sill, Arkona Sea and the Bornholm Basin (Figure 4) show typical

471   absorption characteristics for the individual constituents. CDOM and detritus have high absorption values at the blue

472   end of the spectrum, while phytoplankton shows two maxima, one between 440 nm and 490 nm and a smaller one

473   around 670 nm. There is a clear seasonal pattern for each of the constituents, with spring and summer being peak

474   seasons for phytoplankton blooms, and summer and autumn favouring increased CDOM and detrital absorption.

475   Considerable variability in absorption characteristics is evident between the locations. The highest absorption for all the

476   constituents is seen at the coastal Oder Bank location, which is strongly influenced by riverine inputs from the Oder

477   River. There is a decreasing gradient, especially in CDOM and detrital absorption, moving from the coastal zone to the

478   offshore regions. The summer phytoplankton bloom in the Arkona Sea has a higher peak than the Darß Sill.

479   CDOM, detritus and phytoplankton specific absorption curves intersect around 442 nm, making this an

480   interesting wavelength to explore further with respect to the impact of these constituents on the vertical distribution of

481   absorption and the downward attenuation and irradiance fields.

482   The vertical profiles of phytoplankton, CDOM and detrital absorption at 442 nm (Figure 5) show the vertical

483   extent of water constituent absorption to be the full water column at Oder Bank and Darß Sill and between 15 and 20 m

484   depth at Arkona Sea and Bornholm Basin. In spring and especially in summer, phytoplankton dominate sub-surface

485   absorption at all locations, followed by CDOM and then detrital absorption.

486   The spectrally-resolved surface downward attenuation (K_d) and downward irradiance (E_d) at each of the

487   locations shown in Figure 6 reflect the seasonal impact of the water constituent absorption and solar irradiance.

488   Irradiance at the surface peaks in summer and is at its lowest in winter, as expected. The slight modification of

489   downwelling irradiance intensity in the Baltic Sea depends on atmospheric conditions. Results of direct measurements

490   and local parameterizations of radiative transfer models summarised by Dera and Woźniak (2010) indicate that observed

491   monthly averaged solar irradiance intensities at the sea level in the Baltic Sea are always lower than model estimates

492   based on the clear sky assumption. Atmospheric conditions have a regional and seasonal impact on observed solar

493   irradiance entities e.g. in the southern Baltic Proper and western Baltic Sea, the long-term monthly average for E_d at the

494   surface in May is only 4.8 and 1.8 Wm^{-2}, respectively, lower from E_d intensity observed in June in both regions. This is

495   caused by much lower cloud cover over Baltic Sea observed in May than in June.
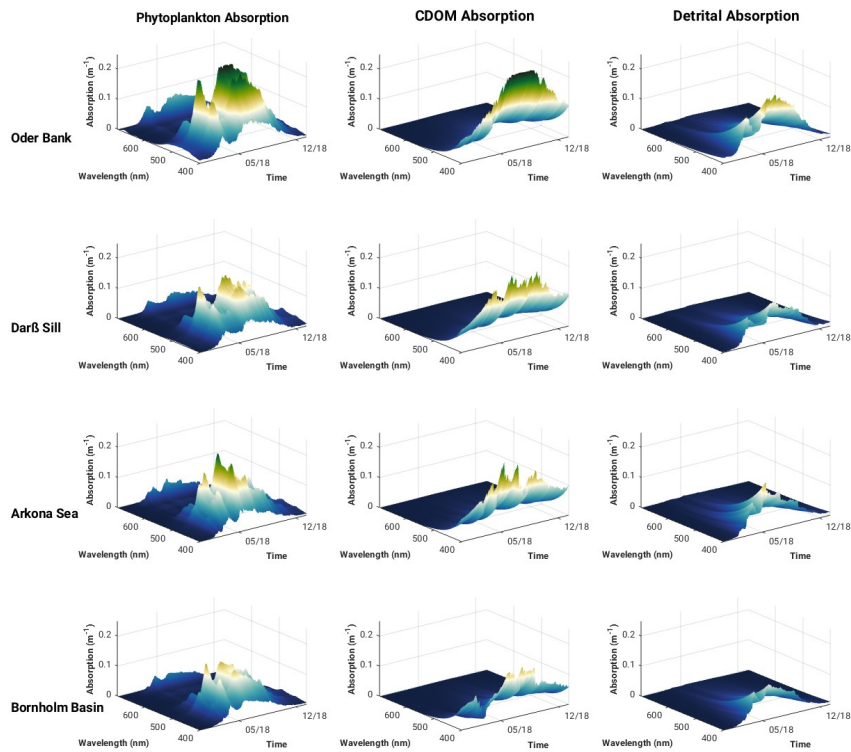
496

497

498   Figure 4: Surface spectral phytoplankton, CDOM and detrital absorption at Oder Bank, Darß Sill, Arkona Sea

499   and Bornholm Basin in 2018 from ROMS-Bio-Optic 3D Western Baltic Sea model experiment.

500

501
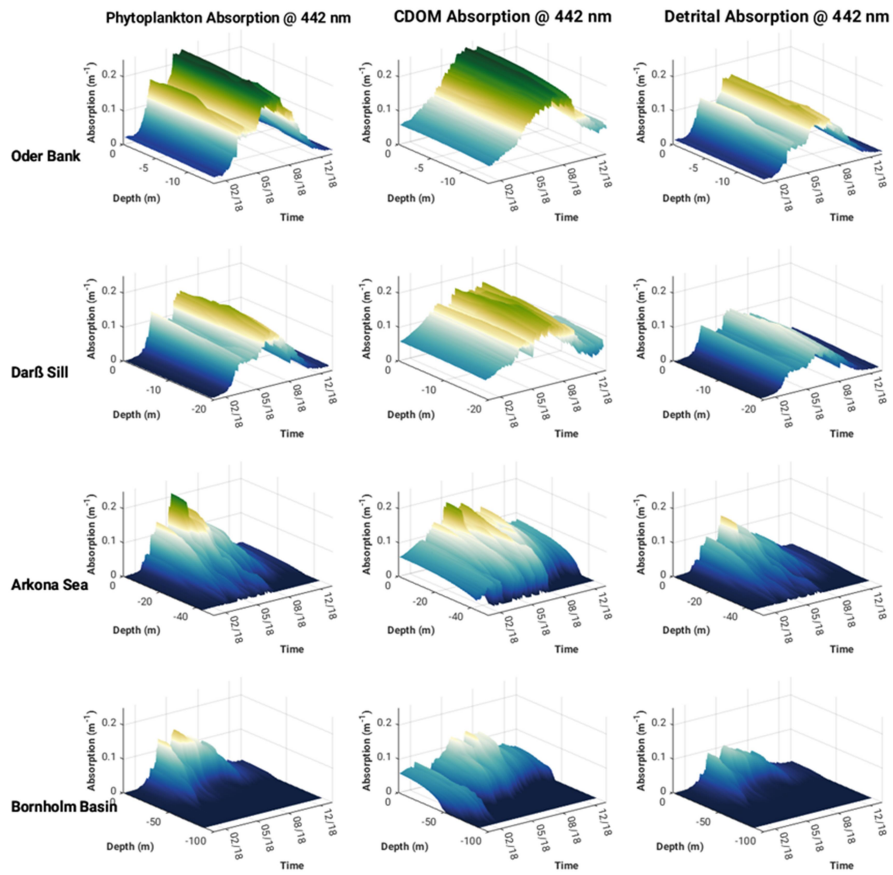
502

503

504   Figure 5: Vertical structure of phytoplankton, CDOM and detrital absorption at 442 nm at Darß Sill, Arkona Sea, Oder

505   Bank and Bornholm Basin in 2018 from ROMS-Bio-Optic 3D Western Baltic Sea model experiment.

506

507

508
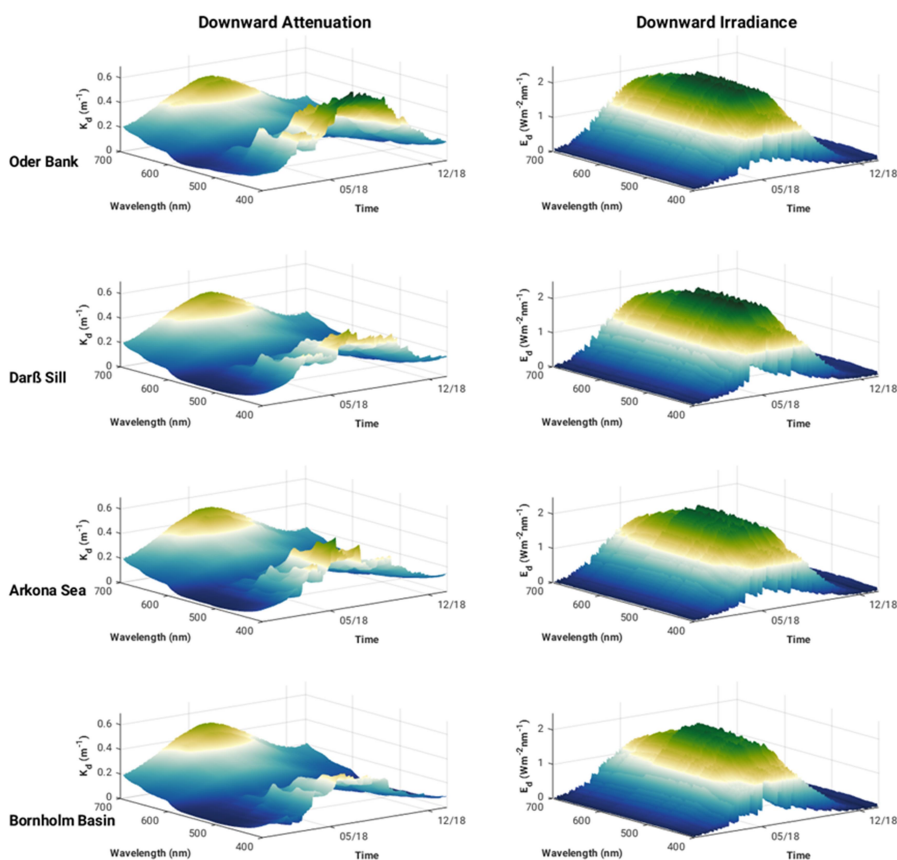
509

510

511   Figure 6: Surface spectral downward diffuse light attenuation and downward irradiance at Oder Bank, Darß

512   Sill, Arkona Sea and Bornholm Basin in 2018 from ROMS-Bio-Optic 3D Western Baltic Sea model experiment.

513

514   Variability in the surface layer attenuation is greatest between 400 and 550 nm, especially during the stratified

515   spring, summer and autumn seasons reflecting the seasonal dynamics of phytoplankton, CDOM and detritus. Vertical

516   profiles of K_d and E_d at 442 nm (Figure 7) show light penetrating deeper in winter, indicating relatively well-mixed

517   (clear) waters, contrasted by seasonally stratified waters in spring, summer and autumn. Variability between the

518   locations is also much higher during these seasons revealing the different influence of constituents at these locations, for

519   example, the impact of the spring and summer phytoplankton blooms at Oder Bank and Arkona Sea on attenuation.

520   (High attenuation values at the red end of the spectrum are mostly related to the absorption of pure water itself).

521
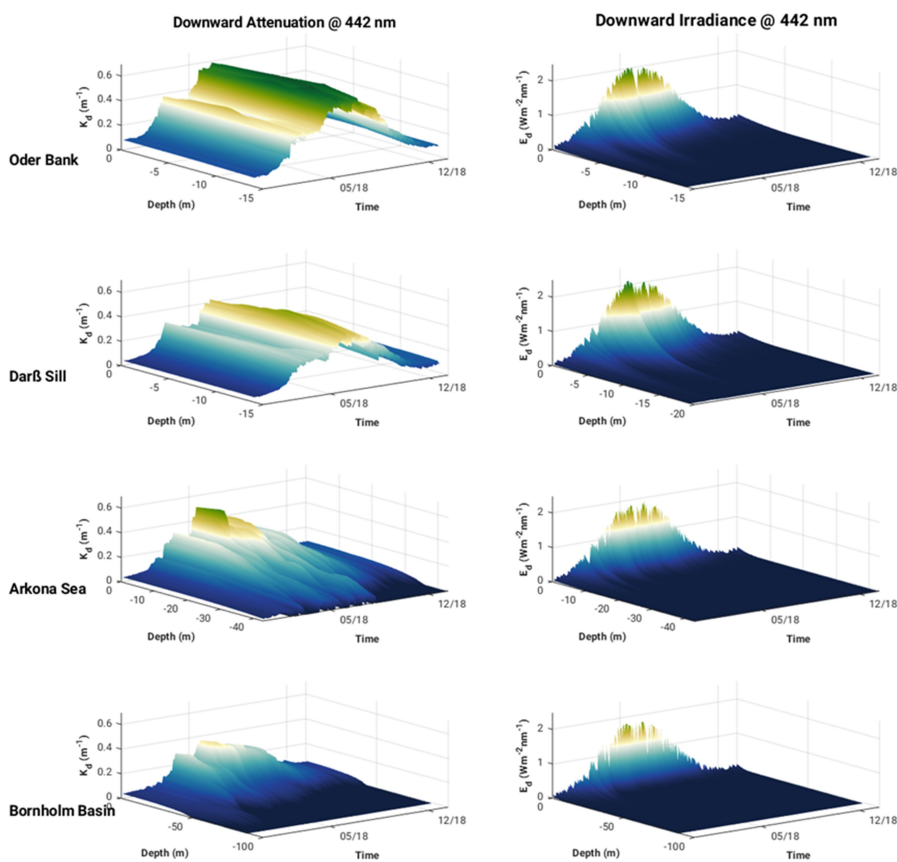
522

523

524   Figure 7: Vertical structure of downward diffuse light attenuation and downward irradiance at 442 nm at Oder

525   Bank, Darß Sill, Arkona Sea and Bornholm Basin in 2018 from ROMS-Bio-Optic 3D Western Baltic Sea model

526   experiment.

527

528   It should be noted that seasonal and spatial variability in the concentration of optically significant water

529   constituents impacts not only the penetration of solar energy into the water column, but also influences the spectral

530   properties of the underwater light field. Elevated absorption by CDOM and phytoplankton pigments in the spring and

531   summer at the Oder Bank, Darß Sill and Arkona Sea causes a red shift in the solar irradiance maximum transmission

532   waveband to 570 nm from 500 nm estimated for the Bornholm Basin (Figure 6). This is consistent with observations

533   reported by Kowalczuk et al. (2005a) who reported a shift in solar irradiance maximum transmission waveband from

534   550 nm in the Baltic Proper to 575 nm in Pomeranian Bay and Gulf in Gdansk. An even bigger shift in the solar

535   irradiance maximum transmission waveband was observed between Atlantic Ocean coastal water off the west coast of

536   Ireland (maximum solar irradiance transmission at 490 nm) and Baltic Sea in Gulf of Gdansk (maximum solar

537   irradiance transmission at 570 nm). This shift was attributed to elevated CDOM absorption, which was c. two times

538   higher in the Baltic Sea compared to coastal Atlantic Ocean, while the chlorophyll-a concentration was at a similar level

539   in both regions (Darecki et al., 2003).

540   3.3 Heating rates and surface heat fluxes

541   The vertical and temporal evolution of water constituent-induced heating rates at each of the locations is shown in

542   Figure 8. Maximum heating rates occur late spring and mid-summer and are between 0.8 and 0.9 K m^{-1}d^{-1} at Oder Bank

543   and between 0.4 and 0.8 K m^{-1}d^{-1} at the other locations. Vertical profiles of two heating rate maxima in May and July

544   indicate approximately 70% of the water constituent-induced heating is contained within the top 5 m, and decreases

545   exponentially to zero by 10 to 15 m depth.

546   We compared the Bio-Optic heating rate estimates at Bornholm Basin with a comparable full radiative transfer

547   calculation by MOMO for the two heating rate maxima events in May and June (Figure 8, bottom right). Bornholm

548   Basin is chosen as the evaluation site for the heating rate calculations because the seasonal cycle of the heat balance

549   there can be approximated as a 1-dimensional balance between the penetration of solar radiation and vertical mixing

550   (Gnanadesikan et al., 2019) and advective and diffusive terms will be relatively small. The main difference between the

551   two calculations, Bio-Optic and MOMO, is that the MOMO takes into account the full directionality of the light field

552   while Bio-Optic does not. There are differences in the seasonal heating rate results between the two approaches but they

553   are not so large. At the surface, the Bio-Optic estimates are 0.3 K m^{-1}d^{-1} smaller in spring and 0.25 K m^{-1}d^{-1} smaller in

554   summer than the MOMO estimates. In the MOMO calculations, most of the water constituent-induced heating (c. 80 %)

555   is contained within the top 2 m, and this decreases exponentially more rapidly than Bio-Optic to zero by 5 m depth.

556   We find that by accounting for the full directionality of the light field, as shown by the case investigated by

557   MOMO, the impact water constituents have on the heating rates is contained within the top 2 to 3 m, consistent with the

558   findings of Soppa et al. (2019). However, MOMO may be overestimating the actual magnitude of water constituent-

559   induced surface heating rates as none of the other physics (i.e. advection, diffusion) and environmental forcing

560   represented in the Bio-Optic experiments, are taken into account in MOMO. It could also be that the algorithm used to

561   calculate K$_d$ in Bio-Optic (Lee et al., 2005) is not optimal for the conditions in the Baltic Sea (we elaborate this point

562   further in the discussion).

563

564
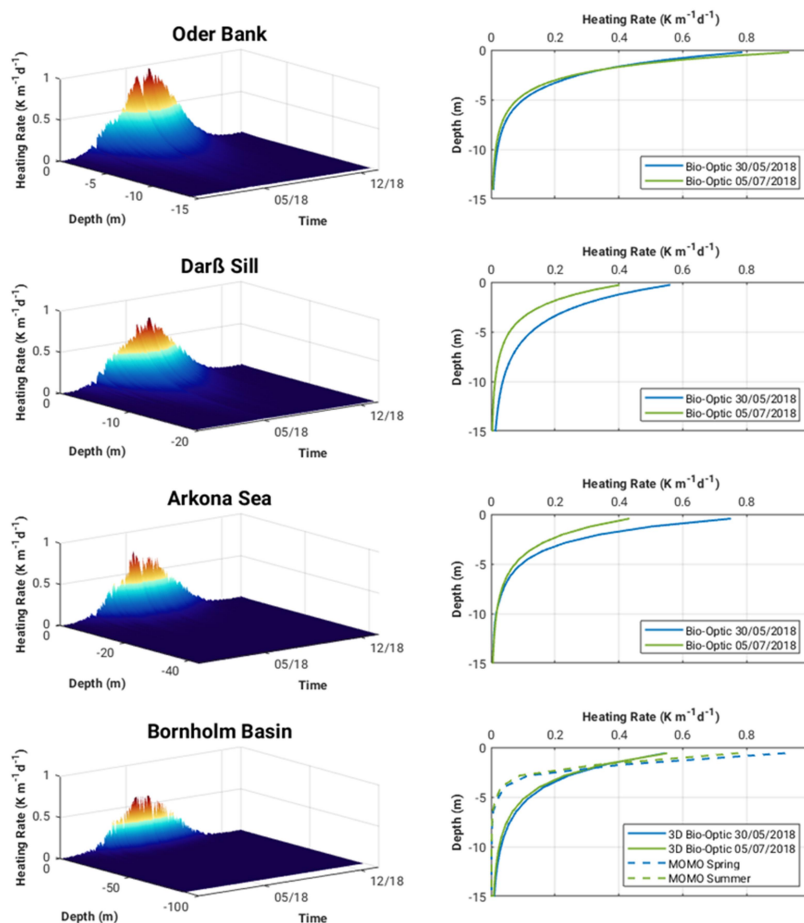
Figure 8: Surface heating rates (left panel) and vertical profiles of two heating rate maxima in May and July 2018 (right panel) for at Oder Bank, Darß Sill, Arkona Sea and Bornholm Basin.

Figure 9 shows the temperature and chlorophyll-a anomalies (biofeed minus nobiofeed experiments) for selected days during the productive period at Bornholm Basin. Accounting for the feedback of OSC-induced heating in the hydrodynamic solution has the effect of increasing the surface layer (c. top 10m) water temperature by between 0.1 and 0.2°C in spring and late summer, and as much as 0.6°C mid-summer. Below the thermocline, the water temperature is cooler by 0.1 to 0.2°C. Differences in the thermal structure when the feedback is accounted for impacts the development, transport and fate of phytoplankton biomass. This consequence is seen in differences in the chlorophyll-a

576 structure at different times during the productive period. In spring, when the upper water column is stratifying, the

577 increase in temperature in the surface layer will stimulate production and increase the absorption of light by

578 phytoplankton, thus, strongly reducing the availability of light below the algae layer. Phytoplankton is restricted within

579 the shallow mixed layer with more availability of light, which will in turn increase surface heating. As nutrients become

580 depleted in the surface layer and the supply of nutrients from deeper waters is inhibited by the stronger thermocline

581 mid-summer, the net effect is less biomass production in the surface layer mid-summer in biofeed compared to

582 nobiofeed. As the water column becomes less stable late August, and nutrients are mixed back into the surface, biomass

583 production is larger again in biofeed compared to nobiofeed.

584
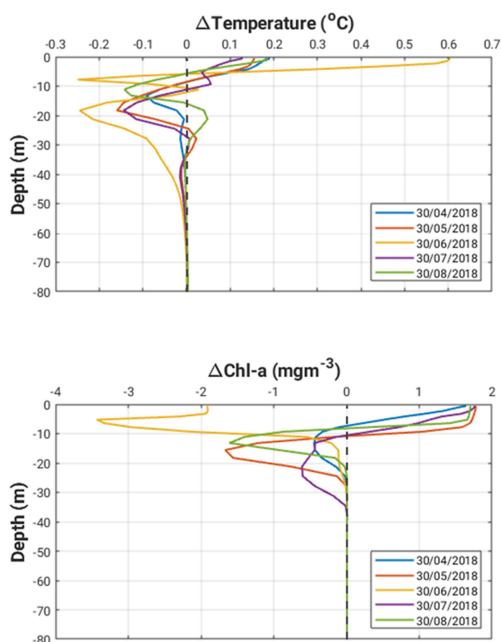
585

586

587 Figure 9: Vertical profiles of temperature and chlorophyll-a anomalies (biofeed minus nobiofeed experiments) during

588 productive period at Bornholm Basin.

589

590 The impact this has on surface heat fluxes during the productive period at Bornholm Basin is shown in Figure

591 10. The increase in OSC-induced surface temperature captured in spring and summer lead to an increase in heat loss to

592 the atmosphere, with the average difference for the period April to September being on the order of 5.2 Wm^{-2}. This is

593 primarily a result of latent (2.6 Wm^{-2}) and sensible (1.7 Wm^{-2}) heat fluxes. Putting this into context with modelled

594   estimates by Omstedt and Nohr (2004) of between 5 and 18 Wm^{-2} for the net annual heat losses in the Baltic Sea,

595   indicates it may be important to consider OSC-induced heating rates in regional heat balance budgets.

596
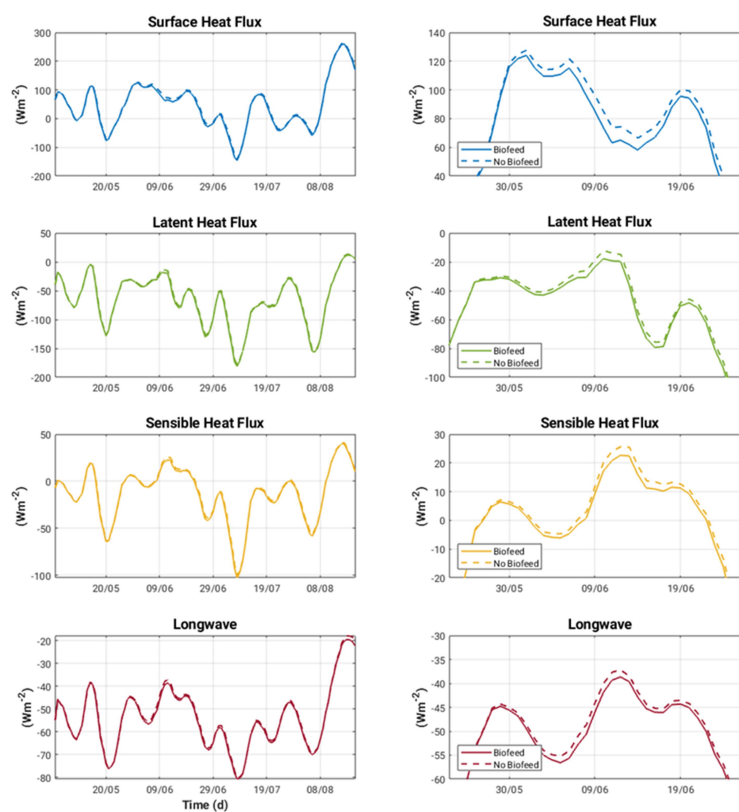
597

598

599   Figure 10: Surface heat fluxes for both biofeed and nobiofeed experiments during productive period at Bornholm Basin.

600

4 Discussion

602   Modelled seasonal and spatial changes in OSCs in the Western Baltic Sea have a small but noticeable impact on

603   radiative heating in surface waters, especially in spring and summer as a consequence of increased absorption of light

604   by phytoplankton and CDOM. Our modelled estimates for 2018 show phytoplankton dominating absorption in spring

605   and summer, as a result of a succession of phytoplankton blooms, and CDOM dominating absorption in summer and

autumn. Simis et al. (2017), found that phytoplankton pigment visibly influences $K_d(675)$ in spring and summer, while absorption by CDOM at 412 nm can account for 38–70 % of the total OSC absorption in the area influenced by the Oder River in autumn. First order variability in CDOM absorption in the Baltic Sea is driven by terrestrial sources. Second order variability is driven by autochthonous DOM production during phytoplankton blooms and photodegradation. The spatial and temporal variability in our modelled OSC absorption at the different locations, especially in spring, summer and autumn, are in good agreement with seasonal observations for different water types in the Southern Baltic Sea reported by Meler et al. (2016a) (See appendix, Figure A1). This is encouraging for future modelling studies of this nature, as more consistent, long term time series of the optical properties of the Baltic Sea are realised e.g. using automated measurement systems such as Bio-Argo floats equipped with a simple spectral radiometer. Such a strategy has been applied with significant success in the Mediterranean Sea (Terzić et al., 2019; Terzić et al., 2021a; Terzić et al., 2021b). We also find it encouraging that the (simplified) Bio-Optic and (full) MOMO radiative transfer heating rate estimates were somewhat comparable and informative. The directionality of the light field appears to be important to understand the depth of influence of water constituent-induced heating rates, while accounting for the spatial and temporal variability in the physics of the environment is important in determining the magnitude of the heating rates. However, we think further work is needed to optimise the Bio-Optic diffuse attenuation coefficient (K_d) algorithm for the Baltic Sea.

K_d which describes the transfer of light energy through the water column, also reflects the seasonal variability of water types, i.e. winter (well-mixed) versus spring, summer and autumn (seasonally stratified) and the influence of constituents in different water types during stratified seasons (i.e. spatial variability). Our results show a gradient in K_d and in heating rates which decreases as you move offshore. In late spring, at the Oder Bank, water constituent contribution to surface heating can be as much as 0.9 K m^{-1}d^{-1}, while at Darß Sill, Arkona Sea and Bornholm Basin, water constituent contribution to surface heating in spring and summer is less, between 0.4 and 0.8 K m^{-1}d^{-1}. Reports on the spectral properties, temporal and spatial variability of the diffuse attenuation coefficient in the Baltic Sea based on field observations are limited and date back to the early 2000s (Kratzer et al. 2003, Lund-Hansen, 2004, Darecki and Stramski 2004, Kowalczuk et al., 2005a, Lee et al., 2005). Darecki and Stramski (2004) have assessed that locally optimised satellite remote sensing algorithms for estimating $K_d(490)$ based on MODIS data yield the least uncertainty compared to other variables e.g. chlorophyll-a. However, information on the full K_d spectrum is needed to assess the individual impact of the most significant optical seawater constituents on surface heating rates. Until recently, the only solution was empirical or semi- analytical modelling based on either remote sensing data (Lee at al. 2005; Löptien and Meier, 2011; Alikas et al., 2015) or in situ measurements of apparent or inherent optical measurements (Gonçalves-Araujo and Markager, 2020). The most accurate estimation of K_d could be achieved by using the semi-analytical model, however, uncertainty in those estimates heavily depends on the local parametrization of the specific inherent optical properties which, in the Baltic Sea regions, have contrasting and highly variable seasonal cycles (Simis et al., 2017). Kratzer and Moore (2018) concluded that the correct choice of the volume scattering phase function in the Baltic Sea

640 determines the accuracy of the prediction of inherent and apparent optical properties in the Baltic Sea region. CDOM

641 and suspended particles are the most significant optical constituents controlling water transparency. CDOM absorption

642 is regulated mostly by riverine discharge especially in coastal waters, however, under certain condition, CDOM

643 absorption in the Baltic Sea is statistically correlated with phytoplankton biomass (Kowalczuk et al., 2006, Meler at al.,

644 2016a). Particulate absorption and scattering is significantly correlated with phytoplankton biomass, which has a well-

645 defined seasonal and spatial pattern in the Baltic Sea (Meler et al., 2016b, Meler at al., 2017). By including a spectrally

646 resolved underwater light field in our model and diagnosing inherent and apparent optical properties, we are able to

647 resolve the full K_d spectrum and better understand the role different OSCs play in determining the temporal and spatial

648 variability in K_d and the impact on heating rates. Further optimisation of the Bio-Optic K_d algorithm for the Baltic Sea

649 is currently in progress.

650   Climate change scenarios for central Europe predict significant change in the precipitation regime, which will

651 be manifested in a shift in the seasonal distribution of precipitation: increased rainfall and decline in snowfall in winter,

652 persistent droughts in summer with episodic intensive thunderstorms (IPCC, 2022). Changes in the precipitation regime

653 coupled with an increase of mean temperatures will significantly impact the outflow of freshwater from the Baltic Sea

654 catchment into the marine basin itself (Meier et al., 2022). We could anticipate that the flux of terrestrial CDOM would

655 be affected most, because currently observed climatic changes in the southern part of Baltic Sea catchment have caused

656 mild winters with reduced numbers of frost days and almost a total reduction in snow fall. As a result, CDOM that was

657 previously immobilised in the frosted ground, streams and rivers, is now being transported to the sea in late winter and

658 spring. In the summer, a deepening minima of flows in rivers reduces CDOM input to Baltic Sea. Recent results by

659 Zabłocka (2017) indicate that the monthly averaged Vistula river flow maximum during the period 1993 to 1998

660 occurred in April, while from 2008 to 2010, this maximum shifted to March. As the Baltic Sea is warming at a rate up to

661 four times the global mean warming rate (Belkin, 2009), we can expect this trend in earlier river flow maxima to

662 continue and a higher contribution of CDOM to the absorption budget in winter and spring, as the chlorophyll-a

663 concentration (phototrophic protists biomass proxy) maximum still occurs in April (Stoń-Egiert and Ostrowska, 2022).

664   Changes in the hydrological regime and a reduction in mineral nutrient input (Łysiak-Pastuszak et al., 2004)

665 have noticeably impacted both phototrophic protists biomass and functional structure. Stoń-Egiert and Ostrowska (2022)

666 have reported a statistically significant decreasing trend of 2.11 % yr^{-1} of the total chlorophyll-a concentrations over last

667 two decades (1999 to 2018), with decreasing pigment markers for such protists groups as diatoms, dinoflagellates,

668 cryptophytes and green algae and an increase of cyanobacteria. As a consequence, primary production in the southern

669 Baltic Sea also declined in the period from 1993 to 2018, compared to its maximum in the late 1980s (Zdun et al., 2021).

670 Kahru et al. (2016) have also reported on changes in the seasonality in the Baltic Sea environment: the cumulative sum

671 of 30,000 $Wm^{-2}d^{-1}$ of surface incoming shortwave irradiance (SIS) was reached 23 days earlier in 2014 compared to 3

672 decades earlier; the period of the year when the sea surface temperature was at least 17°C has almost doubled (from 29

673 days in 1982 to 56 days in 2014); the period when $K_d(490)$ was over 0.4 m^{-1} increased from about 60 days in 1998 to

674   240 days in 2013 (quadrupled); the period when satellite-estimated chlorophyll of at least 3 mgm^{-3} has doubled from

675   110 days in 1998 to 220 days in 2013 and the timing of both the phytoplankton spring and summer blooms has

676   advanced, with the annual chlorophyll maximum that in the 1980s corresponded to the spring diatom bloom in May has

677   now shifted to the summer cyanobacteria bloom in July. It is interesting to note that we found two OSC-induced heating

678   rate maxima in May and July in our model results which coincide with two observed marine heatwave events. At Darß

679   Sill and Arkona Sea, these heating rate maxima were larger in May, by 0.18 and 0.35 K m^{-1}d^{-1}, respectively compared to

680   July, while at Oder bank the heating rate maxima was larger in July by 0.1 K m^{-1}d^{-1}.

681   **5 Conclusions**

682   Heating rates due to absorption of short wave radiation (UV-VIS) in the Western Baltic Sea are controlled by the

683   combined effects of the seasonal solar cycle and the concentration and distribution of OSCs. The intensity of radiative

684   energy reaching the sea surface is locally modified by radiative transfer through the atmosphere, which is mostly

685   controlled by cloudiness whose long term climatology minimum is observed in May (Dera and Woźniak, 2010). Further

686   modulation of heating rates in the Western Baltic Sea in UV and VIS spectral domains is dependent on water

687   transparency which is a complex function of the magnitude and seasonal cycles of inherent optical properties and the

688   directionality of the light field. Our study found that in 2018 the combined effect of CDOM and particulate absorption

689   on surface heating rates in the Western Baltic Sea could reach up to 0.4 to 0.8 K d^{-1}, during the productive period April

690   to September, and is relevant from the surface down to 2-5 m depth. Moreover, this modelled OSC-induced surface

691   warming results in a mean loss of heat (c. 5 Wm^{-2}) from the sea to the atmosphere, primarily in the form of latent and

692   sensible heat fluxes, which may be significant for regional heat balance budgets. Two way coupling with the

693   atmosphere is not included in our experiment, but we expect this would modulate (decrease) the magnitude of the net

694   loss of heat to the atmosphere.

695   Anticipated and recently observed changes in phytoplankton functional types and their seasonal pattern and

696   CDOM terrestrial input patterns due to global warming will further modulate the spatial and temporal pattern of heating

697   rates in the Baltic Sea. Observed changes in the quantity and quality of CDOM, the composition and concentration of

698   phytoplankton functional types and photosynthetic pigments and thus changes to the optical properties of the Baltic Sea,

699   need to be communicated to coupled hydrodynamic-biogeochemical models such that the consequences of radiative

700   feedbacks can be better understood and better predictions of the future Baltic Sea environment can be made. Further

701   improvements to coupled hydrodynamic and ecological models are heavily dependent on the correct parameterization

702   of the downwelling irradiance diffuse attenuation coefficient K_d, which requires a proper understanding of the seasonal

703   and spatial variability of the optical properties in different water types. This work highlights the importance of K_d as a

704   bio-optical driver: K_d provides a pathway to estimating heating rates and connects biological activity with energy fluxes.

705

706   **Appendix A: Model versus in situ and remotely sensed observations**
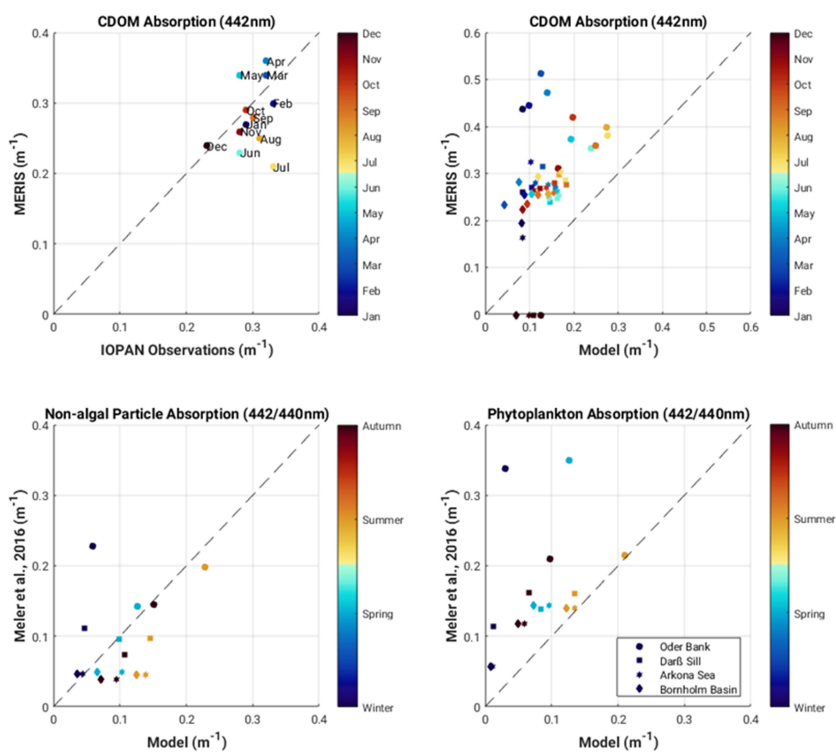
707

708

709   Figure A1: (a) MERIS and in situ monthly climatology of surface CDOM absorption (mean value calculated over

710   Western Baltic Sea region shown in Figure 1); (b) mean monthly surface CDOM absorption at model stations and

711   matching MERIS locations; seasonal mean surface non-algal particle absorption (CDOM+detritus) (c) and

712   phytoplankton absorption (d) at model stations compared with similar water type values found in Meler et al. (2016).

713

714

715

Code Availability:

The ROMS-BioOptic model code used in this study can be accessed at https:// www.myroms.org. The MOMO model code is available upon request from Jürgen Fischer, juergen.fischer@fu-berlin.de

Data availability:

The version of the Bio-Optic model code used to produce the results in this study, including initial conditions, river and boundary forcing as well as selected model output used for analysis and producing figures are archived on Zenodo (10.5281/zenodo.7215110 – reserved).

The atmospheric forcing data can be acquired for scientific research purposes upon request from Ulf Gräwe (ulf.graewe@io-warnemuende.de).

The MERIS FRS L2 CDOM absorption monthly climatology for the Western Baltic Sea used in this study is archived on Zenodo (10.5281/zenodo.7224656 - reserved).

The in situ CDOM absorption data can be acquired for scientific research purposes upon request from Piotr Kowalczuk (piotr@iopan.pl).

Author contributions:

BC conceived the study, extended the ECOSIM model code and set up the regional deployment of ROMS-BioOptic in the Western Baltic Sea. BC also performed all simulations and analysis, and wrote the manuscript with input from all co-authors. PK provided the in situ CDOM absorption data used in the study and made significant contributions to the manuscript. LK and JF provided support setting up the MOMO model code and expertise on radiative transfer theory in the ocean. UG provided model grid bathymetry, atmospheric forcing, as well as initial and boundary conditions. UG and JW provided support setting up and troubleshooting the regional deployment of ROMS in the Western Baltic Sea.

Competing interests:

The authors declare that they have no conflict of interest.

Acknowledgements:

BC was supported by funding from the German Research Foundation (Grant No. CA 1347/2-1, 2018 to 2021, Temporary Position for Principal Investigator). PK was supported by the Statutory Research Program at the Institute of Oceanology Polish Academy of Sciences no. II.5 and partially by project "Oceanographic Data and Information System", eCUDO.pl (contract no. POPC.02.03.01-IP.01-00-0062/18) co-financed from European Regional Development Fund, Digital Poland Operational Program, 2.2 Priority Axis. The authors gratefully acknowledge the computing time granted by the Resource Allocation Board and provided on the supercomputer Lise and Emmy at NHR@ZIB and NHR@Göttingen as part of the NHR infrastructure. The calculations for this research were conducted with computing resources under the project ID bek00027. BC would like to thank the Free University of Berlin (FUB) for hosting her during the project. The following individuals are also gratefully acknowledged: Jakob Röhrenbach for compiling the MERIS CDOM absorption data archive, Rene Preusker for providing additional expertise on radiative transfer theory, Jan El Kassar for providing data management support, Hernan Arango and David Robertson at Rutgers University for providing support with ROMS code development and troubleshooting, Thomas Neumann from the Leibniz Institute for Baltic Sea Research for providing the biogeochemical river forcing data used in the study and Frank Fell for making some very helpful comments on an earlier version of the manuscript.

References

Aas, E.: Two-stream irradiance model for deep waters, Appl. Opt., 26, 2095 – 2101, https://doi.org/10.1364/AO.26.002095, 1987.

Ackleson, S., Balch, W. and Holligan, P.: Response of water-leaving radiance to particulate calcite and chlorophyll *a* concentrations: A model for Gulf of Maine coccolithophore blooms, Journal of Geophysical Research, 99(C4), https://doi.org/10.1029/93JC02150, 1994.

Alikas, K., Kratzer, S., Reinart, A., Kauer, T. and Paavel, B.: Robust remote sensing algorithms to derive the diffuse attenuation coefficient for lakes and coastal waters, Limnology and Oceaongraphy: Methods, 13(8), 402 – 415, https://doi.org/10.1002/lom3.10033, 2015.

Alikas, K. and Kratzer, S.: Improved retrieval of Secchi depth for optically-complex waters using remote sensing data, Ecological Indicators, 77, 218 – 227, https:/doi.org/10.1016/J.ECOLIND.2017.02.007, 2017.

Belkin, I.: Rapid warming of large marine ecosystems, Progress in Oceanography, 81(1-4), 207 – 213, https://doi.org/10.1016/J.POCEAN.2009.04.011, 2009.

Bennartz, R. and Fischer, J.: A modified k-distribution approach applied to narrow band water vapour and oxygen absorption estimates in the near infrared, Journal of Quantitative Spectroscopy and Radiative Transfer, 539 – 553, https://doi.org/10.1016/S0022-4073(99)00184-3, 2000.

Bennartz, R. and Fischer, J.: Retrieval of columnar water vapour over land from backscattered solar radiation using the Medium Resolution Imaging Spectrometer, Remote Sensing of Environment, 78, 274 – 283, https://doi.org/10.1016/S0034-4257(01)00218-8, 2001.

Bissett, W., Walsh, J., Dieterle, D. and Carder, K.: Carbon cycling in the upper waters of the Sargasso Sea: I. Numerical simulation of differential carbon and nitrogen fluxes, Deep Sea Research Part I: Oceanographic Research Papers, 46(2), 205 – 269, https://doi.org/10.1016/S0967-0637(98)00062-4, 1999a.

Bissett, W., Walsh, J., Dieterle, D. and Carder, K.: Carbon cycling in the upper waters of the Sargasso Sea: II. Numerical simulation of apparent and inherent optical properties, Deep Sea Research Part I: Oceanographic Research Papers, 46(2), 271 – 317, https://doi.org/ 10.1016/S0967-0637(98)00063-6, 1999b.

Cahill, B., Schofield, O., Chant, R., Wilkin, J., Hunter, E., Glenn, S. and Bissett, P.: Dynamics of turbid buoyant plumes and the feedbacks on near-shore biogeochemistry and physics, Geophysical Research Letters, 35(19), 1 – 6, https://doi.org/.1029/2008GL033595, 2008.

Cahill, B., Wilkin, J., Fennel, K., Vandemark, D. and Friedrichs, M.: Interannual and seasonal variabilities in air-sea CO_2 fluxes along the U.S. eastern continental shelf and their sensitivity to increasing air temperatures and variable winds, Journal of Geophysical Research: Biogeosciences, 121(2), 295 – 311, https://doi.org/ 10.1002/2015JG002939, 2016.

Darecki, M., Weeks, A., Sagan, S., Kowalczuk, P. and Kaczmarek, S.: Optical characteristics of two contrasting Case 2 waters and their influence on remote sensing algorithms, Continental Shelf Research, 23(3-4), 237 – 250, https://doi.org/10.1016/S0278-4343(02)00222-4, 2003.

Darecki, M. and Stramski, D.: An evaluation of MODIS and SeaWiFS bio-optical algorithms in the Baltic Sea, Remote Sensing of Environment, 89(3), 326 – 350, https://doi.org/10.1016/J.RSE.2003.10.012, 2004.

Dera, J., and Woźniak, B.: Solar radiation in the Baltic Sea, Oceanologia, 52(4), 533–582, 2010.

Dickey, T. and Falkowski, P.: Solar energy and its biological-physical interactions in the sea, in *The Sea*, 12, eds. Allan R. Robinson, James J. McCarthy and Brian J. Rothschild, John Wiley & Sons, NY, ISBN 0-471-18901-4, 2002.

Doerffer, R. and Schiller, H.: The MERIS case 2 water algorithm, International Journal of Remote Sensing, 28(3-4), 517 – 535, https://doi.org/10.1080/01431160600821127, 2007.

Dutkiewicz, S., Hickman, A., Jahn, O., Gregg, W., Mouw, C. and Follows, M.: Capturing optically important constituents and properties in a marine biogeochemical and ecosystem model, Biogeosciences, 12(14), 4447 – 4481, https://doi.org/10.5194/bg-12-4447-2015, 2015.

Fell, F. and Fischer, J.: Numerical simulation of the light field in the atmosphere-ocean system using the matrix-operator method, Journal of Quantitative Spectroscopy and Radiative Transfer, 69(3), 351 – 388, https://doi.org/10.1016/S0022-4073(00)00089-3, 2001.

851 Jolliff, J. and Smith, T.: Biological modulation of upper ocean physics: Simulating the biothermal feedback effect in
852   Monterey Bay, California, Journal of Geophysical Research: Biogeosciences, 119(5), 703 – 721,
853   https://doi.org/10.1002/2013JG002522, 2014.

854 Karhu, M., Elmgren, R. and Savchuk, O.: Changing seasonality of the Baltic Sea, Biogeosciences, 13(4), 1009 – 1018,
855   https://doi.org/10.5194/bg-13-1009-2016, 2016.

856 Kim, G., Pradal, M. and Gnanadesikan, A.: Quantifying the biological impact of surface ocean light attenuation by
857   colored detrital matter in an ESM using a new optical parameterization, Biogeosciences, 12(16), 5199 – 5132,
858   https://doi.org/10.5194/bg-12-5119-2015, 2015.

859 Kim, G., Gnanadesikan, A. and Pradal, M.: Increased surface ocean heating by colored detrital matter (CDM) linked to
860   greater northern hemisphere ice formation in the GFDL CM2Mc ESM, Journal of Climate, 29(24), 9063 – 9076,
861   https://doi.org/ 10.1175/JCLI-D-16-0053.1, 2016.

862 Kim, G., Gnanadesikan, A. Del Castillo, C. and Pradal, M.: Upper ocean cooling in a coupled climate model due to light
863   attenuation by yellowing materials, Geophysical Research Letters, 45(12), 6134 – 6140,
864   https://doi.org/10.1029/2018GL077297, 2018.

865 Kim, G., St-Laurent, P., Friedrichs, M. and Mannino, A.: Impacts of water clarity variability on temperature and
866   biogeochemistry in the Chesapeake Bay, Estuaries and Coasts, 43(8) 1973 – 1991,
867   https://doi.org/10.1007/s12237-020-00760-x, 2020.

868 Kowalczuk, P.: Seasonal variability of yellow substance absorption in the surface layer of the Baltic Sea, Journal of
869   Geophysical Research - Oceans, 104(C12), 30 047-30 058, 1999.

870 Kowalczuk, P. And Kaczmarek, S.: Analysis of temporal and spatial variability of "yellow substance" absorption in the
871   Southern Baltic, Oceanologia, 38(1), 3-32, 1996.

872 Kowalczuk, P., Sagan, S., Olszewski, J., Darecki, M. and Hapter,R.: Seasonal changes in selected optical parameters in
873   the Pomeranian Bay in 1996-1997, Oceanologia, 41(3), 309-334, 1999.

874 Kowalczuk, P., Olszewski, J., Darecki, M. and Kaczmarek, S.: Empirical relationships between Coloured Dissolved
875   Organic Matter (CDOM) absorption and apparent optical properties in Baltic Sea waters, International Journal of
876   Remote Sensing, 26(2), 345-370, 2005a.

877 Kowalczuk, P., Stoń-Egiert, J., Cooper, W. J., Whitehead, R. F. And Durako, M. J.: Characterization of Chromophoric
878   Dissolved Organic Matter (CDOM) in the Baltic Sea by Excitation Emission Matrix fluorescence spectroscopy.
879   Marine Chemistry, 96, 273-292, 2005b.

880 Kowalczuk P., Stedmon, C. A. and Markager, S.: Modelling absorption by CDOM in the Baltic Sea from season,
881   salinity and chlorophyll, Marine Chemistry, 101, 1-11, 2006.

882 Kowalczuk, P., Sagan, S., Zablocka, M. and Borzycka, K.: Mixing anomaly in deoxygenated Baltic Sea deeps indicates
883   benthic flux and microbial transformation of chromophoric and fluorescent dissolved organic matter, Estuarine,
884   Coastal and Shelf Science, 163, 206 – 217, https://doi.org/10.1016/j.ecss.2015.06.027, 2015.

885 Kratzer, S., Hakansson, B. and Sahlin, C.: Assessing Secchi and photic zone depth in the Baltic sea from satellite data,
886   Ambio, 32(8), 577 – 585, https://www.jstor.org/stable/4315443, 2003.

887 Kratzer, S. and Moore, G.: Inherent optical properties of the Baltic Sea in comparison to other seas and oceans, Remote
888   Sensing, 10(3), https://doi.org/10.3390/rs10030418, 2018.

889 Kritten, L., Preusker, R. and Fischer, J.: A new retrieval of sun-induced chlorophyll fluorescence in water from ocean
890   colour measurements applied on OLCI L-1b and L-2, Remote Sensing, 12(23), 1 – 24,
891   https://doi.org/10.3390/rs12233949, 2020.

892 Lee, Z., Du, K. and Arnone, R.: A model for the diffuse attenuation coefficient of downwelling, Journal of Geophysical
893   Research: Oceans, 110(2) 1 – 10, https://doi.org/10.1029/2004JC002275, 2005.

894 Lewis, M., Carr, M., Feldman, G., Esaias, W. and McClain, C.: Influence of penetrating solar radiation on the heat
895   budget of the equatorial Pacific Ocean, Nature, 347, https://doi.org/https://doi.org/10.1038/347543a0, 1990.

896 Lindstrot, R., Preusker, R. and Fischer, J.: The retrieval of land surface pressure from MERIS measurements in the
897   oxygen a band, Journal of Atmospheric and Oceanic Technology, 26(7), 1367 – 1377,
898   https://doi.org/10.1175/2009JTECHA1212.1, 2009.

Löptien, U. and Meier, H.E.M.: The influence of increasing water turbidity on the sea surface temperature in the Baltic sea: A model sensitivity study, Journal of Marine Systems, 88(2), 323 – 331, https://doi.org/10.1016/J.JMARSYS.2011.06.001, 2011.

Lund-Hansen, L.: Diffuse attenuation coefficients K_d(PAR) at the estuarine North Sea-Baltic Sea transition: time-series, partitioning, absorption and scattering, Estuarine, Coastal and Shelf Science, 61(2), 251 – 259, https://doi.org/10.1016/J.ECSS.2004.05.004, 2004.

Łysiak-Pastuszak, E., Drgas, N. and Piatkowska, Z.: Eutrophication in the Polish coastal zone: the past, present status and future scenarios, Mar. Pollut. Bull. 49 (3), 186–195, https://doi.org/10.1016/j.marpolbul.2004.02.007, 2004.

Manizza, M., Quere, C., Watson, A. and Buitenhuis, E.: Bio-optical feedbacks among phytoplankton, upper ocean physics and sea-ice in a global model, Geophysical Research Letters, 32(5), 1 – 4, https://doi.org/10.1029/2004GL020778, 2005.

Manizza, M., Quere, C., Watson, A. and Buitenhuis, E.: Ocean biogeochemical response to phytoplankton-light feedback in a global model, Journal of Geophysical Research: Oceans, 113(10), https://doi.org/10.1029/2007JC004478, 2008.

Meier, H. E. M., Kniebusch, M., Dieterich, C., Gröger, M., Zorita, E., Elmgren, R., Myrberg, K., Ahola, M. P., Bartosova, A., Bonsdorff, E., Börgel, F., Capell, R., Carlén, I., Carlund, T., Carstensen, J., Christensen, O. B., Dierschke, V., Frauen, C., Frederiksen, M., Gaget, E., Galatius, A., Haapala, J. J., Halkka, A., Hugelius, G., Hünicke, B., Jaagus, J., Jüssi, M., Käyhkö, J., Kirchner, N., Kjellström, E., Kulinski, K., Lehmann, A., Lindström, G., May, W., Miller, P. A., Mohrholz, V., Müller-Karulis, B., Pavón-Jordán, D., Quante, M., Reckermann, M., Rutgersson, A., Savchuk, O. P., Stendel, M., Tuomi, L., Viitasalo, M., Weisse, R., and Zhang, W.: Climate change in the Baltic Sea region: a summary, Earth Syst. Dynam., 13, 457–593, https://doi.org/10.5194/esd-13-457-2022, 2022.

Meler, J., Ostrowska, M., Stoń-Egiert, J. and Zabłocka., M.: Seasonal and spatial variability of light absorption by suspended particles in the southern Baltic: A mathematical description, Journal of Marine Systems, 170, 68 – 87, https://doi.org/10.1016/J.JMARSYS.2016.10.011, 2017.

Meler, J., Ostrowska, M. and Stoń-Egiert, J.: Seasonal and spatial variability of phytoplankton and non-algal absorption in the surface layer of the Baltic, Estuarine, Coastal and Shelf Science, 180, 123 – 135, https://doi.org/10.1016/J.ECSS.2016.06.012, 2016a.

Meler, J., Kowalczuk, P., Ostrowska, M., Zabłocka, M. and Zdun, A.: Parameterization of the light absorption properties of chromophoric dissolved organic matter in the Baltic Sea and Pomeranian lakes, Ocean Science, 12(4), 1013 – 1032, https://doi.org/ 10.5194/os-12-1013-2016, 2016b.

Morel, A. and Prieur, L.: Analysis of variations in ocean color, Limnology and Oceanography, 2(4), 709 – 722, https://doi.org/10.4319/lo.1977.22.4.0709, 1977.

Morel, A.: Optical modelling of the upper ocean in relation to its biogenous matter content (Case I waters), Journal of Geophysical Research, 93, 749 – 768, https://doi.org/10.1029/JC093iC09p10749, 1988.

Morel, A. and Antoine, D.: Heating rate within the upper ocean in relation to its bio-optical state, Journal of Physical Oceanography, 24, 1652 – 1665, https://doi.org/10.1175/1520-0485(1994)024%3C1652:HRWTUO%3E2.0.CO;2, 1994.

Murtugudde, R., Beauchamp, J., McClain, C., Lewis, M. and Busalacchi, A.: Effects of penetrative radiation on the upper tropical ocean circulation, Journal of Climate, 15, 470 – 486, https://doi.org/10.1175/1520-0442(2002)015%3C0470:EOPROT%3E2.0.CO;2, 2002

Neumann, T., Siegel, H. and Gerth, M.: A new radiation model for Baltic Sea ecosystem modelling, Journal of Marine Science, 152, 83 – 91, https://doi.org/10.1016/j.jmarsys.2015.08.001, 2015.

Neumann, T., Koponen, S., Attila, J., Brockmann, C., Kallio, K., Kervinen, M., Mazeran, C., Müller, D., Philipson, P., Thulin, S., Väkevä. S. and Ylöstalo, P.: Optical model for the Baltic Sea with an explicit CDOM state variable: A case study with Model ERGOM (version 1.2), Geoscientific Model Development, 14(8), 5049 – 5062, https://doi.org/10.5194/gmd-14-5049-2021, 2021.

Ohlmann, J., Siegel, D. and Gautier, C.: Ocean mixed layer radiant heating and solar penetration: A global analysis, Journal of Climate, 9, https://doi.org/10.1175/1520-0442(1996)009%3C2265:OMLRHA%3E2.0.CO;2, 1996.

Ohlmann, J., Siegel, D. and Washburn, L.: Radiant heating of the western equatorial Pacific during TOGA-COARE, Journal of Geophysical Research: Oceans, 103(C3), 5379 – 5395, https://doi.org/ 10.1029/97jc03422, 1998.

Ohlmann, J., Siegel, D. and Mobley, C.: Ocean radiant heating. Part I: Optical Influences, Journal of Physical Oceanography, 30, 1833 – 1848, https://doi.org/10.1175/1520-0485(2000)030%3C1833:ORHPIO%3E2.0.CO;2, 2000.

Ohlmann, J. and Siegel, D.: Ocean radiant heating. Part II: Parameterizing solar radiation transmission through the upper ocean, Journal of Physical Oceanography, 30, 1833 – 1848, https://doi.org/10.1175/1520-0485(2000)030%3C1849:ORHPIP%3E2.0.CO;2, 2000.

Omstedt, A. and Nohr, C.: Calculating the water and heat balances of the Baltic Sea using ocean modelling and available meteorological, hydrological and ocean data, Tellus A: Dynamic Meteorology and Oceanography, 56(4), 400 – 414, https://doi.org/10.3402/tellusa.v56i4.14428, 2004.

Oschlies, A.: Feedbacks of biotically induced radiative heating on upper-ocean heat budget, circulation and biological production in a coupled ecosystem-circulation model, Journal of Geophysical Research: Oceans, 109(12), 1 – 12, https://doi.org/10.1029/2004JC002430, 2004.

Paulson, C and Simpson, J.: Irradiance measurements in the upper ocean, Journal of Physical Oceanography, 7, 952 – 956, https://doi.org/10.1175/1520-0485(1977)007%3C0952:IMITUO%3E2.0.CO;2, 1977.

Pefanis, V., Losa, S. N., Losch, M., Janout, M. A. and Bracher, A: Amplified Arctic surface warming and sea ice loss due to phytoplankton and colored dissolved material, Geophysical Research Letters, 47, e2020GL088795, https://doi.org/10.1029/2020GL088795 , 2020.

Röhrenbach, J.: Seasonal variability in the absorption of coloured dissolved organic matter (CDOM) in the western and southern Baltic Sea, Bachelor Thesis, Department of Earth Sciences, Free University Berlin, November 2019.

Sathyendranath, S. and Platt, T.: The spectral irradiance field at the surface and in the interior of the ocean: A model for applications in oceanography and remote sensing, Journal of Geophysical Research, 93(C8), https://doi.org/10.1029/JC093iC08p09270, 1988.

Sathyendranath, S., Prieur, L and Morel, A.: A three-component model of ocean colour and its application to remote sensing of phytoplankton pigments in coastal waters, International Journal of Remote Sensing, 10(8) 1373 – 1394, https://doi.org/ 10.1080/01431168908903974, 1989.

Shchepetkin, A. and McWilliams, J.: The regional oceanic modelling system (ROMS): A split-explicit, free-surface, topography-following-coordinate ocean model, Ocean Modelling, 9(4), 347 – 404, https://doi.org/10.1016/j.ocemod.2004.08.002, 2005.

Siegel, H., Gerth, M., Ohde, T. and Heene, T.: Ocean colour remote sensing relevant water constituents and optical properties of the Baltic Sea, International Journal of Remote Sensing, 26(2), 315 – 330, https://doi.org/10.1080/01431160410001723709, 2005.

Simis, S., Ylöstalo, P., Kallio, K., Spilling, K. and Kutser, T.: Contrasting seasonality in optical biogeochemical properties of the Baltic Sea, PLOS ONE, 12(4), https://doi.org/10.1371/journal.pone.0173357, 2017.

Simpson, J. and Dickey, T.: Alternative parameterizations of downward irradiance and their dynamical significance, Journal of Physical Oceanography, 11, 876 – 882, https://doi.org/10.1175/1520-0485(1981)011%3C0876:APODIA%3E2.0.CO;2, 1981.

Skákala, J., Bruggeman, J., Ford, D., Wakelin, S., Akpınar, A., Hull, T., Kaiser, J., Loveday, B.R., O'Dea, E., Williams, C.A.J. and Ciavatta, S.: The impact of ocean biogeochemistry on physics and its consequences for modelling shelf seas, Ocean Modelling, 172, https://doi.org/10.1016/j.ocemod.2022.101976, 2022.

Soppa, A., Pefanis, V., Hellmann, S., Losa, S., Hölemann J., Janout, M., Martynov, F., Heim, B., Dinter, R., Rozanov, V. and Bracher, A.: Assessing the influence of water consitutents on the radiative heating of Laptev Sea shelf waters, Frontiers in Marine Science, https://doi.org/10.3389/fmars.2019.00221, 2019.

Stedmon, C., Markager, S. and Kaas, H.: Optical properties and signatures of chromophoric dissolved organic matter (CDOM) in Danish coastal waters, Estuarine, Coastal and Shelf Science, 51(2), 267 – 278, https://doi.org/10.1006/ecss.2000.0645, 2000.

Stoń-Egiert, J. and Ostrowska, M.: Long-term changes in phytoplankton pigment contents in the Baltic Sea: Trends and spatial variability during 20 years of investigations, Continental Shelf Research 236 (2022) 104666, doi:10.1016/j.csr.2022.104666, 2022.

Taucher, J. and Oschlies, A.: Can we predict the direction of marine primary production change under global warming? Geophysical Research Letters, 38(2), https://doi.org/10.1029/2010GL045934, 2011.

Terzic, E., Lazzari, P., Organelli, E., Solidoro, C., Salon, S., D'Ortenzio, F. and Conan, P.: Merging bio-optical data from Biogeochemical-Argo floats and models in marine biogeochemistry, Biogeosciences, 16(12), 2527 – 2542, https://doi.org/10.1029/2021JC017690, 2019.

Terzic, E., Miro, A., Organelli, E., Kowalczuk, P., D'Ortenzio, F and Lazzari, P.: Radiative transfer modelling with Biogeochemical –Argo float data in the Mediterranean Sea, Journal of Geophysical Research: Oceans, 126(10), https://doi.org/10.1029/2021JC017690, 2021a.

Terzic, E., Salon, S., Cossarini, G., Solidoro, C., Teruzzi, A., Miro, A. and Lazzari, P.: Impact of interannually variable diffuse attenuation coefficients for downwelling irradiance on biogeochemical modelling, Ocean Modelling, 161, https://doi.org/10.1016/J.OCEMOD.2021.101793, 2021b.Wetzel, P., Maier-Reimer, E., Botzet, M., Jungclaus, J., Keenlyside, N. and Latif, M.: Effects of ocean biology on the penetrative radiation in a coupled climate model, Journal of Climate, 19, 3973 – 3987, https://doi.org/10.1175/JCLI3828.1, 2006.

Wilkin, J., Zhang, W. G., Cahill, B. and Chant, R. C.: Integrating coastal models and observations for studies of ocean dynamics, observing systems and forecasting, In Operational Oceanography in the 21st Century, A. Schiller and G. Brassington (Eds.), Springer, doi: 10.1007/978-94-007-0332-2_19, 2011.

Wohlers, J., Engel, A., Breithaupt, P., Jü, K., Hoppe, H., Sommer, U. and Riebesell, U.: Changes in biogenic carbon flow in response to sea surface warming, PNAS, 106 (17) 7067-7072, https://doi.org/10.1073/pnas.0812743106, 2009.

Zaneveld, J. and Spinrad, R.: An arc tangent model of irradiance in the sea, Journal of Geophysical Research, 85(C9), https://doi.org/ 10.1029/JC085iC09p04919, 1980.

Zängl, G., Reinert, D., Rípodas, P. and Baldauf, M: The ICON (ICOsahedral Non-hydrostatic) modelling framework of DWD and MPI-M: Description of the non-hydrostatic dynamical core, Quarterly Journal of the Royal Meteorological Society, 141(687), 563–579, https://doi.org/10.1002/qj.2378, 2015.

Zdun, A., Stoń -Egiert, J., Ficek, D and Ostrowska, M.: Seasonal and Spatial Changes of Primary Production in the Baltic Sea (Europe) Based on in situ Measurements in the Period of 1993–2018, Front. Mar. Sci. 7:604532., doi: 10.3389/fmars.2020.604532, 2021.

Zhang, T., Fell, F., Zhi-Shen, L., Preusker, R., Fischer, J. and Ming.Xia, H.: Evaluating the performance of artificial neural network techniques for pigment retrieval from ocean color in Case I waters, Journal of Geophysical Research, 108(C9), https://doi.org/10.1029/2002JC001638, 2003.